Conclusions and perspectives

The current reports by Rentschler et al. and Aanhaanen et al. clearly demonstrate that accessory pathway formation underlying ventricular preexcitation arises as a consequence of erroneous development of the AV canal myocardium. A hierarchical network of transcription factors, including *Tbx2/3/5*, *Nkx2.5*, *GATA4*, and *Msx2*, governs normal development of the AV canal under the regulation of Notch and BMP signaling (10). Contrary to previous reports demonstrating that Notch signaling restricts BMP2 and Tbx2/3 to the AV canal during early embryogenesis (16, 17), the expression level of BMP2 was unchanged in Notch1-activated mice (1). Our understanding of the pathophysiology of ventricular preexcitation will be broadened by further characterization of the genetic program for AV canal development.

Acknowledgments

This work was supported in part by grants from Japan Society for the Promotion of Science (KAKENHI 20390218, 21229010); Health and Labor Sciences Research grants (to I. Komuro and H. Akazawa); and grants from Astellas Foundation for Research on Metabolic Disorders, The Uehara Memorial Foundation, The Ichiro Kanehara Foundation, Mochida Memorial Foundation for Medical and Pharmaceutical Research, and Suzuken Memorial Foundation (to H. Akazawa).

Address correspondence to: Issei Komuro, Department of Cardiovascular Medicine, Osaka University Graduate School of Medicine, 2-2 Yamadaoka, Suita, Osaka 565-0871, Japan. Phone: 81.6.6879.3631; Fax: 81.6.6879.3639; E-mail: komuro-tky@umin.ac.jp.

1. Rentschler S, et al. Notch signaling regulates murine atrioventricular conduction and the formation of accessory pathways. *J Clin Invest.* 2011;121(2):525–533.
2. Aanhaanen WTJ, et al. Defective Tbx2-dependent patterning of the atrioventricular canal myocardium causes accessory pathway formation in mice. *J Clin Invest.* 2011;121(2):534–544.
3. Blair E, et al. Mutations in the gamma(2) subunit of AMP-activated protein kinase cause familial hypertrophic cardiomyopathy: evidence for the central role of energy compromise in disease pathogenesis. *Hum Mol Genet.* 2001;10(11):1215–1220.
4. Gollob MH, et al. Identification of a gene responsible for familial Wolff-Parkinson-White syndrome. *N Engl J Med.* 2001;344(24):1823–1831.
5. Arad M, Seidman CE, Seidman JG. AMP-activated protein kinase in the heart: role during health and disease. *Circ Res.* 2007;100(4):474–488.
6. Arad M, et al. Transgenic mice overexpressing mutant PRKAG2 define the cause of Wolff-Parkinson-White syndrome in glycogen storage cardiomyopathy. *Circulation.* 2003;107(22):2850–2856.
7. Sidhu JS, et al. Transgenic mouse model of ventricular preexcitation and atrioventricular reentrant tachycardia induced by an AMP-activated protein kinase loss-of-function mutation responsible for Wolff-Parkinson-White syndrome. *Circulation.* 2005;111(1):21–29.
8. Wessels A, Markman MW, Vermeulen JL, Anderson RH, Moorman AF, Lamers WH. The development of the atrioventricular junction in the human heart. *Circ Res.* 1996;78(1):110–117.
9. Kolditz DP, et al. Epicardium-derived cells in development of annulus fibrosis and persistence of accessory pathways. *Circulation.* 2008;117(12):1508–1517.
10. Hatcher CJ, Basson CT. Specification of the cardiac conduction system by transcription factors. *Circ Res.* 2009;105(7):620–630.
11. Aanhaanen WT, et al. The Tbx2+ primary myocardium of the atrioventricular canal forms the atrioventricular node and the base of the left ventricle. *Circ Res.* 2009;104(11):1267–1274.
12. Aanhaanen WT, et al. Developmental origin, growth, and three-dimensional architecture of the atrioventricular conduction axis of the mouse heart. *Circ Res.* 2010;107(6):728–736.
13. Tallini YN, et al. Imaging cellular signals in the heart in vivo: Cardiac expression of the high-signal Ca2+ indicator GCaMP2. *Proc Natl Acad Sci U S A.* 2006;103(12):4753–4758.
14. Kolditz DP, et al. Persistence of functional atrioventricular accessory pathways in postseptated embryonic avian hearts: implications for morphogenesis and functional maturation of the cardiac conduction system. *Circulation.* 2007;115(1):17–26.
15. Hahurij ND, et al. Accessory atrioventricular myocardial connections in the developing human heart: relevance for perinatal supraventricular tachycardias. *Circulation.* 2008;117(22):2850–2858.
16. Rutenberg JB, Fischer A, Jia H, Gessler M, Zhong TP, Mercola M. Developmental patterning of the cardiac atrioventricular canal by Notch and Hairy-related transcription factors. *Development.* 2006;133(21):4381–4390.
17. Kokubo H, Tomita-Miyagawa S, Hamada Y, Saga Y. Hesr1 and Hesr2 regulate atrioventricular boundary formation in the developing heart through the repression of Tbx2. *Development.* 2007;134(4):747–755.
18. Ma L, Lu MF, Schwartz RJ, Martin JF. Bmp2 is essential for cardiac cushion epithelial-mesenchymal transition and myocardial patterning. *Development.* 2005;132(24):5601–5611.
19. Harrelson Z, et al. Tbx2 is essential for patterning the atrioventricular canal and for morphogenesis of the outflow tract during heart development. *Development.* 2004;131(20):5041–5052.
20. Anderson RH, Ho SY. Anatomy of the atrioventricular junctions with regard to ventricular preexcitation. *Pacing Clin Electrophysiol.* 1997;20(8 pt 2):2072–2076.

Growing a tumor stroma: a role for granulin and the bone marrow

Andrew Bateman

Endocrine Research Laboratory, Royal Victoria Hospital, Research Institute of the McGill University Health Centre, Montreal, Quebec, Canada.

The tumor stroma is critical in cancer progression; understanding its formation is therefore important biologically and therapeutically. In this issue of the *JCI*, Elkabets et al. report on the generation of data in mice that lead them to propose that certain tumors can stimulate the growth of a second otherwise quiescent or indolent tumor in the same animal by stimulating stromal formation. Granulin-expressing Sca^+Kit^- hematopoietic progenitor cells in the bone marrow of the tumor host were required to mediate this effect. These data shed new light on the importance of the bone marrow in tumor growth and the role of granulin in carcinogenesis.

Conflict of interest: The author has declared equity in Neurodyn Inc.

Citation for this article: *J Clin Invest.* doi:10.1172/JCI46088.

Background: systemic tumor instigation

The reactive (or desmoplastic) stroma is an aberrant fibrous tissue that surrounds cancer cells (1). It is formed from fibroblasts, adipocytes, inflammatory cells, and vascular cells and is further characterized by the presence of myofibroblasts (1). Myofibroblasts display properties not usually associated with fibroblasts in healthy tissue, such as the expression of αSMA, and secrete high levels of matrix proteins such as collagen I (1). The molecular properties of tumor stroma are predictive of disease outcome (2), with the stromal cells, in particular the myofibroblasts, stimulating tumor growth, invasion, and metastasis (1). For example, molecular crosstalk between cancer cells

Circulation Journal
Official Journal of the Japanese Circulation Society
http://www.j-circ.or.jp

EDITORIAL

Costarring Statins With ARBs

– Going to Be a Smash Hit? –

Shoji Sanada, MD, PhD; Issei Komuro, MD, PhD

Based on the accumulating evidence, some major pharmacological strategies for improving the morbidity and mortality of patients with chronic heart failure (HF) have been recently proposed. To date, according to numerous previous clinical studies, renin–angiotensin system (RAS) inhibition and β-adrenergic blockade are the most assured and reliable options,[1] so they are the first-line in the current therapeutic guidelines for chronic HF[2] and most patients are strongly recommended to take as high doses of these medicines as they can tolerate.[3] However, despite the continuous intensive research that has proposed various kinds of mechanistic insights as putative candidates, we do not have any other efficacious pharmacological strategies in daily clinical practice that might be as potent and sufficient to parallel those 2 standard options for coping with HF,[4] which has been a huge problem over the past 2 decades.

Article p 589

Recently, hydroxymethyl glutaryl coenzyme-A reductase inhibitors (statins), which primarily modify the endogenous cholesterol profile, have emerged as a hopeful candidate for a novel therapeutic option for treating HF,[5,6] pending investigation of the mechanisms underlying their clinical benefits.

In this issue of the Journal, Maejima et al[7] intriguingly report from the results of their randomized study involving 32 patients (the HF-costar trial) that the additional use of simvastatin exerted enhanced benefits, such as further improvement of NYHA classification and significant reduction in plasma B-type natriuretic peptide (BNP) levels, together with a trend toward increased recovery of the echocardiographic ejection fraction, in patients with mild to moderate chronic HF treated with losartan, which alone also brought recovery in part.

Their most noteworthy finding is that the improvements in patient status were independent of any hemodynamic or inflammatory change, except a mild reduction in the plasma cholesterol level, by simvastatin. In their study, the final blood pressure of 122/73 in the losartan group, which remained unchanged throughout the study, strongly supports the pleiotropic benefits of RAS inhibition, apart from blood pressure reduction, as implicated by many previous experimental studies.[8] Actually, the administered dose of losartan in this study was designed to be 25–50 mg/day, which is indeed the standard therapeutic regimen in this patient population. However, we are approved to prescribe the higher dose of 100 mg/day in the same population in daily clinical practice. Moreover, the benefits of RAS inhibition in previous clinical trials were often accompanied by significant blood pressure reduction,[9] and some recent studies reported that higher doses of RAS-inhibiting agents provided a better outcome when safe and tolerable[3] in patients with cardiovascular diseases. Therefore, it is arguable whether the present dose of losartan was optimal for maximal therapeutic potential, not underpowered.

Likewise, we cannot directly distinguish the combined effects of losartan with simvastatin from the effects of simvastatin alone because of the absence of the wing of "treated alone" in this study. Some recent small clinical trials[5,6] demonstrated substantial improvement in cardiac status evaluated by NYHA classification, echocardiographic cardiac function and plasma BNP level, the same parameters used in this study, to a similar extent by additional treatment with simvastatin in patients with chronic HF. Despite the limitation of the number of patients, a direct comparison would have provided more details regarding separate and synergistic effects.

As to the mechanistic insights, Node et al[5] proposed elimination of inflammatory reactions, represented by reduced plasma levels of TNF-α or IL-6, as the potential benefits of simvastatin therapy; however, in this study the plasma hsCRP levels remained unchanged. Because this study is missing a direct evaluation of TNF-α or IL-6, we cannot tell whether hsCRP is directly linked with those 2 cytokines, which might imply unknown "co-starring" beneficial mechanisms other than CRP-related inflammatory cascades. For example, if TNF-α was selectively affected by additional treatment with statins in this study, it might lead to activation of p38MAPK and JNK, which potently modulate the pathophysiology of HF,[10] but that seems somewhat different from the cardioprotective mechanisms induced by RAS-inhibitory agents.[8]

Furthermore, it might also be the case that nitric oxide-dependent mechanisms and anti-oxidant effects, which are also supposed to be pleiotropic cardioprotective cascades induced by both RAS-inhibitory agents and statins,[1] played a role in this situation. However, it remains controversial whether these cardioprotective cascades might be prevailing similarly in the clinical setting, and whether these are common or distinct among RAS-inhibitory agents and statins. Therefore,

Received December 14, 2010; accepted December 14, 2010; released online January 24, 2011
Department of Cardiovascular Medicine, Osaka University Graduate School of Medicine, Suita (S.S., I.K.), Osaka University Health Care Center, Suita (S.S.), Japan
Mailing address: Shoji Sanada, MD, PhD, Department of Cardiovascular Medicine, Osaka University Graduate School of Medicine, 2-2 Yamada-oka, Suita 565-0871, Japan. E-mail: s-sanada@cardiology.med.osaka-u.ac.jp
ISSN-1346-9843 doi:10.1253/circj.CJ-10-1251

further evaluation of the same population is awaited.

In addition, the drug-selective property of statins for downstream modulation and cardioprotection might differ in terms of magnitude,[11] which might also be the case with RAS inhibitory agents. Further investigations using various class-wide alternatives to identify their class-sensitive as well as drug-specific benefits in patients with HF, and to seek the best combination of the specific drugs, are awaited.

Meanwhile, another remarkable finding is that having only 16 patients in each wing was sufficient to reach statistical significance. Although the present study,[7] as well as previous studies,[5,6] show a remarkable reduction in plasma BNP levels and a substantial recovery of cardiac function in such small study populations, they are hardly reflected in the large clinical trials, which have been mostly negative for drastic changes in plasma BNP level or overall primary outcomes.[12] One reason for the discrepancy is that the patients' characteristics and group composition would be different from those in the practical large cohorts, as was pointed out in the report from the J-CARE-GENERAL study.[13] Another possible reason is that the major determinants of primary outcome would be significantly biased to cerebrovascular events, arrhythmic events or cancers, which do not correlate with plasma BNP level or cardiac contractile function, but frequently occur in the clinical setting and is unfortunately usually beyond the analyses in a small population.

We hope that direct interventions on each potential target will uncover the beneficial mechanisms for preventing HF in the real world in the near future.

References

1. Landmesser U, Wollert KC, Drexler H. Potential novel pharmacological therapies for myocardial remodeling. *Cardiovasc Res* 2009; **81:** 519–527.
2. Hunt SA; American College of Cardiology; American Heart Association Task Force on Practice Guidelines. ACC/AHA 2005 guideline update for the diagnosis and management of chronic heart failure in the adult: A report of the American College of Cardiology/American Heart Association Task Force on Practice Guidelines. *J Am Coll Cardiol* 2005; **46:** e1–e82.
3. McMurray JJ, Ostergren J, Swedberg K, Granger CB, Held P, Michelson EL, et al. Effects of candesartan in patients with chronic heart failure and reduced left-ventricular systolic function taking angiotensin-converting-enzyme inhibitors: The CHARM-Added trial. *Lancet* 2003; **362:** 767–771.
4. Dorn GW 2nd. Novel pharmacotherapies to abrogate postinfarction ventricular remodeling. *Nat Rev Cardiol* 2009; **6:** 283–291.
5. Node K, Fujita M, Kitakaze M, Hori M, Liao JK. Short-term statin therapy improves cardiac function and symptoms in patients with idiopathic dilated cardiomyopathy. *Circulation* 2003; **108:** 839–843.
6. Gürgün C, Ildizli M, Yavuzgil O, Sin A, Apaydin A, Cinar C, et al. The effects of short term statin treatment on left ventricular function and inflammatory markers in patients with chronic heart failure. *Int J Cardiol* 2008; **123:** 102–107.
7. Maejima Y, Nobori K, Ono Y, Adachi S, Suzuki J, Hirao K, et al for the Heart Failure by Coadministration of Statin and Angiotensin-II Receptor Blocker (HF-COSTAR) Trial Investigators. Synergistic effect of combined HMG-CoA reductase inhibitor and angiotensin-II receptor blocker therapy in patients with chronic heart failure: The HF-COSTAR trial. *Circ J* 2011; **75:** 589–595.
8. Sanada S, Kitakaze M, Node K, Takashima S, Ogai A, Asanuma H, et al. Differential subcellular actions of ACE inhibitors and AT1 blockers on cardiac remodeling induced by chronic inhibition of nitric oxide synthesis in rats. *Hypertension* 2001; **38:** 404–411.
9. Konstam MA, Rousseau MF, Kronenberg MW, Udelson JE, Melin J, Stewart D, et al. Effects of the angiotensin converting enzyme inhibitor enalapril on the long-term progression of left ventricular dysfunction in patients with heart failure: SOLVD Investigators. *Circulation* 1992; **86:** 431–438.
10. Zhang D, Gaussin V, Taffet GE, Belaguli NS, Yamada M, Schwartz RJ, et al. TAK1 is activated in the myocardium after pressure overload and is sufficient to provoke heart failure in transgenic mice. *Nat Med* 2000; **6:** 556–563.
11. Sanada S, Asanuma H, Minamino T, Node K, Takashima S, Okuda H, et al. Optimal windows of statin use for immediate infarct-limitation: 5'-nucleotidase as another downstream molecule of phosphatidylinositol-3 kinase. *Circulation* 2004; **110:** 2143–2149.
12. Kjekshus J, Apetrei E, Barrios V, Böhm M, Cleland JG, Cornel JH, et al. Rosuvastatin in older patients with systolic heart failure. *N Engl J Med* 2007; **357:** 2248–2261.
13. Tsutsui H, Tsuchihashi-Makaya M, Kinugawa S, Goto D, Takeshita A; JCARE-GENERAL Investigators. Characteristics and outcomes of patients with heart failure in general practices and hospitals. *Circ J* 2007; **71:** 449–454.

MOLECULAR AND CELLULAR BIOLOGY, Mar. 2011, p. 1054–1065 Vol. 31, No. 5
0270-7306/11/$12.00 doi:10.1128/MCB.00732-10

Increased Akt-mTOR Signaling in Lung Epithelium Is Associated with Respiratory Distress Syndrome in Mice[▽]

Hiroyuki Ikeda,[1,2] Ichiro Shiojima,[1,3] Toru Oka,[1,3] Masashi Yoshida,[1] Koji Maemura,[4] Kenneth Walsh,[5] Takashi Igarashi,[2] and Issei Komuro[1,3]*

Department of Cardiovascular Science and Medicine, Chiba University Graduate School of Medicine, Chiba, Japan[1]; Department of Pediatrics, University of Tokyo Graduate School of Medicine, Tokyo, Japan[2]; Department of Cardiovascular Medicine, Osaka University Graduate School of Medicine, Suita, Japan[3]; Department of Cardiovascular Medicine, Nagasaki University Graduate School of Biomedical Sciences, Nagasaki, Japan[4]; and Molecular Cardiology, Whitaker Cardiovascular Institute, Boston University School of Medicine, Boston, Massachusetts[5]

Received 24 June 2010/Returned for modification 31 August 2010/Accepted 17 December 2010

Pregnancy in women with diabetes is associated with a higher risk of perinatal complications. In particular, infants of diabetic mothers frequently suffer from respiratory distress syndrome (RDS), which is a leading cause of death in preterm infants and is considered to be primarily due to hyperinsulinemia in infants in response to maternal hyperglycemia. To elucidate the mechanism of how insulin signaling induces RDS, bronchoalveolar epithelium-specific Akt1 transgenic (TG) mice were generated. Akt1 overexpression in fetal lung epithelium resulted in RDS in preterm infants born by Caesarean section at embryonic day 18.5 (E18.5). The expression levels of hypoxia-inducible factor 2α (HIF-2α) and its target vascular endothelial growth factor (VEGF) were downregulated in the lung of Akt1 TG mice. Inhibition of the Akt-mammalian target of rapamycin (mTOR) signaling axis by rapamycin restored the expression of VEGF and improved the lung pathology of Akt1 TG pups. Rapamycin also attenuated the RDS phenotype in wild-type mice delivered preterm at E17.5. In cultured lung epithelial cells, insulin reduced VEGF expression and transcriptional activity of HIF-2 on *VEGF* promoter in an mTOR-dependent manner. Thus, aberrant activation of the Akt-mTOR pathway in lung epithelium plays a causal role in the pathogenesis of infant RDS, presumably through downregulation of HIF-2-dependent VEGF expression in the lung.

Pregnancy in women with diabetes is associated with a higher risk of perinatal complications. The estimated prevalence rate of gestational diabetes is approximately 4% and is considered to represent 90% of all cases of diabetes diagnosed during pregnancy (2). Moreover, pregnant women with type 2 diabetes are increasing in number in line with the rapid increase in the prevalence of type 2 diabetes in all age groups (9). Infants of diabetic mothers frequently suffer from macrosomia, neonatal hypoglycemia, cardiomegaly, respiratory difficulties, and other congenital anomalies (3, 5, 14, 21), which are considered to be primarily due to hyperinsulinemia in infants in response to maternal hyperglycemia. Respiratory distress syndrome (RDS) is one of the most clinically significant perinatal complications, with high morbidity and mortality (19, 22). RDS is caused by attenuated production of pulmonary surfactant, a mixture of phospholipids and surfactant-associated proteins that covers the alveolar surface and prevents alveolar collapse by reducing the surface tension of the air-water interface (12). Because pulmonary surfactant is specifically produced by type II lung epithelial cells, attenuated production of pulmonary surfactant is considered to be due to impaired differentiation and/or maturation of type II lung epithelial cells (31). Reduced expression of surfactant-associated proteins was observed in fetuses of streptozotocin-induced diabetic rats or in insulin-treated human fetal lung explants (8, 10, 11), suggesting that hyperactivation of insulin signaling in the lung plays a causal role in the pathogenesis of RDS of infants having a diabetic mother.

Phosphatidylinositol 3-kinase (PI3K) is activated by insulin and is responsible for most of the metabolic actions of insulin. PI3K also controls cell growth, differentiation, survival, and protein synthesis (28). The involvement of the PI3K pathway in RDS was suggested by a previous report showing that bronchoalveolar-specific deletion of *Pten* in mice led to upregulation of the PI3K pathway in the lung and resulted in RDS associated with marked hyperplasia of alveolar epithelial cells, increased numbers of bronchoalveolar stem cells (BASCs), and impaired production of surfactant proteins (SPs) (33). It was also shown that genetic ablation of hypoxia-inducible factor 2α (HIF-2α) causes RDS due to downregulation of vascular endothelial growth factor (VEGF) expression in the lung and that intratracheal VEGF administration stimulates maturation of type II lung epithelial cells (4). However, the downstream effectors of PI3K that cause RDS and the mechanistic link between the PI3K pathway and HIF-2-dependent VEGF expression in the lung have been elusive.

Using bronchoalveolar epithelium-specific Akt1 transgenic (TG) mice, we show here that aberrant activation of the Akt-mammalian target of rapamycin (mTOR) pathway in lung epithelium plays a causal role in the pathogenesis of infant RDS. We also provide evidence suggesting that sustained Akt-mTOR activation induces RDS through downregulation of HIF-2-dependent VEGF expression in the lung.

* Corresponding author. Mailing address: Department of Cardiovascular Medicine, Osaka University Graduate School of Medicine, 2-2 Yamadaoka, Suita 565-0871, Japan. Phone: 81 6 6879 3631. Fax: 81 6 6879 3639. E-mail: komuro-tky@umin.ac.jp.

▽ Published ahead of print on 28 December 2010.

MATERIALS AND METHODS

Animals and DOX administration. SP-C-rtTA TG mice expressing the reverse tetracycline transactivator (rtTA) protein under the control of the human surfactant protein-C promoter (pro-SP-C) on the FVB/N background were de-

scribed previously (23, 29) and were purchased from the Jackson Laboratory. These mice were crossed with Tet-myrAkt1 TG mice (25) harboring a myristoylated Akt1 (myrAkt1) transgene under the control of multimerized *tetO* sequences maintained on a mixed background of FVB/N, C57BL/6J, and 129Sv. For myrAkt1 expression, dams were treated with doxycycline (DOX) in drinking water from embryonic day 0.5 (E0.5) at a final concentration of 0.5 mg/ml (25, 29). Respiratory rate was measured by visual inspection of the movements of thorax and abdomen for 1 min. All animal procedures were performed with the approval of the Institutional Animal Care and Use Committee of Chiba University.

Histological analysis and immunohistochemistry. Lungs were formalin fixed without constant pressure inflation and embedded in paraffin for histological analyses. Serial sections of 4 μm were stained with hematoxylin and eosin (HE) for morphological analysis, periodic acid-Schiff (PAS) for detection of glycogen-rich cells, and Masson's trichrome (MT) for detection of fibrosis. Aerated lung area and alveolar septal thickness were measured in toluidine blue-stained sections using ImageJ software (4). Aerated lung area was measured in 10 visual fields for each animal. Septal thickness was measured at 10 points in each visual field, and 10 visual fields for each animal were used for the measurement. The size and number of saccules were measured in PAS-stained sections using ImageJ software. The size of 10 saccules was measured in each visual field, and 10 visual fields for each animal were used for the analysis. Saccular number was counted in 10 visual fields for each animal. Immunohistochemistry was performed using an avidin-biotin-horseradish peroxidase detection system with Nidiaminobenzidine (DAB) (ABC kit; Vector Laboratories) and Nuclear Fast Red as a counterstain. The antibodies used were hemagglutinin (HA), pro-SP-C, Clara cell 10-kDa protein (CC10), aquaporin-5 (AQP5), VEGF (Santa Cruz Biotechnology), and calcitonin gene-related peptide (CGRP; BioMol).

Fluorescence imaging. A BZ-9000 (Keyence) microscope was used for fluorescence imaging. Paraffin-embedded lung sections were incubated with isolectin B4-fluorescein isothiocyanate (FITC) conjugate (Sigma) to detect endothelial cells and with wheat germ agglutinin-tetramethyl rhodamine isothiocyanate (TRITC) conjugate (Sigma) to counterstain the cell membrane. Vascular cell counts with three replications were performed with BZ application software (Keyence), and the median value was used for each sample.

Western blot analysis. Total protein lysate was extracted from lung tissue, and SDS-PAGE was performed as described previously (26). The antibodies used were HA, total Akt1, total S6 kinase (S6K), SP-A, pro-SP-C, AQP5, CC10, VEGF, glyceraldehyde-3-phosphate dehydrogenase (GAPDH; Santa Cruz Biotechnology), phospho-Akt (Ser473), phospho-S6K1 (Thr389), phospho-S6 (Ser235/236), total S6, phospho-glycogen synthase kinase 3β (phospho-GSK3β) (Ser9), phospho-FOXO3a (318/321), total FOXO3a (Cell Signaling Technology), SP-B, SP-D (Chemicon/Millipore), and HIF-2α (Novus Biologicals). Densitometric analysis was performed using ImageJ.

Mouse model of preterm infants. Pups were collected by Caesarean section at E18.5 for Akt1 TG mice and at E17.5 for wild-type ICR mice (4, 20). The umbilical cord was cut, amniotic fluid and membranes were removed from the mouth and nose, and body temperature was kept at 37°C.

Administration of rapamycin. Rapamycin (LC Laboratories) was prepared in the solvent containing 0.2% sodium carboxymethylcellulose and 0.25% polysorbate-80 in water (24, 25). Rapamycin (1 mg/kg of body weight/day) or vehicle was administered subcutaneously to dams.

Reporter gene assays. Luciferase assays were performed essentially as previously described (18). The plasmids used were VEGF reporter plasmid (pGL2hVEGF) and the expression vectors for HIF-1α (phHIF-1α), HIF-2α (phEP-1), and ARNT (phARNT). A549 cells were transfected with the plasmids indicated in the Fig. 8 legend and treated with 250 μM $CoCl_2$ to mimic hypoxic condition.

Statistical analysis. Data are expressed as means ± standard errors of the means (SEM). Statistical significance between two groups was determined with a Student's *t* test or χ^2 test. Probability values of <0.05 were considered to be statistically significant.

RESULTS

Generation of bronchoalveolar epithelium-specific Akt1 TG mice. Two lines of TG mice (Tet-myrAkt1 and SP-C-rtTA) were used to generate bronchoalveolar epithelium-specific Akt1 TG mice (Fig. 1A). The Tet-myrAkt1 TG line harbors an active form of the Akt1 transgene (myrAkt1) under the control of multimerized tetracycline operator (*tetO*) sequences (25), and the SP-C-rtTA TG line expresses the reverse tetracycline transactivator (rtTA) in respiratory epithelial cells driven by human surfactant protein-C (SP-C) promoter (23, 29). DOX enables rtTA binding to *tetO* sequences by inducing its conformational change. Therefore, DOX treatment of double-TG (DTG) mice harboring both transgenes induces transcription of the myrAkt1 gene in lung epithelial cells (Fig. 1A). Mating of SP-C-rtTA mice with Tet-myrAkt1 mice resulted in the generation of mice with four different genotypes (wild type, Tet-myrAkt1 single TG, SP-C-rtTA single TG, and DTG) at the expected frequencies. Western blot analysis of lung lysates harvested at postnatal day 0 (P0) revealed that the transgene product detected by anti-HA blotting was observed in the lung of DTG mice treated with DOX (Fig. 1B). The induced expression of myrAkt1 was associated with a marked increase in phosphorylation levels of several downstream effectors such as S6K1, S6, and glycogen synthase kinase-3 (GSK3), but not FOXO3 (Fig. 1B). Because it was reported that treatment of SP-C-rtTA mice with DOX may exert toxic effects on alveolar epithelial cells (20), the phenotype of DOX-treated SP-C-rtTA single-TG mice was carefully compared with littermates of other genotypes (wild type, Tet-myrAkt1 single TG, and DTG). However, although there was an obvious lung phenotype in DTG mice (described in detail below), no apparent abnormality was observed in mice with other genotypes under our experimental conditions (Fig. 1C and D). We therefore used DOX-treated single-TG littermates as controls in this study.

Akt activation in lung epithelial cells *in utero* results in transient tachypnea associated with delayed maturation of the lung. Activation of Akt signaling in the lung was achieved by DOX treatment of dams starting at embryonic day 0.5 (E0.5). When analyzed at P0, DTG pups were viable and exhibited no cyanosis or growth retardation (Fig. 2A). Postnatal growth of DTG animals was also comparable to that of control mice. However, DTG mice at P0 exhibited significant tachypnea (Fig. 2B) and various histological abnormalities such as markedly reduced aerated space, increased atelectasis, bronchiolar hyperplasia, impaired thinning of the alveolar septa, and abundant PAS-positive glycogen stores (Fig. 2C to E). Since PAS-positive glycogen is normally converted to surfactant phospholipids in mature epithelial cells, these observations suggest that the differentiation of lung epithelial cells is impaired by aberrant activation of Akt signaling. Of note, these histological findings were improved spontaneously at P2 (Fig. 2C to E). Although mild elastic fiber deposition was observed at P2, no such pathology was evident at the age of 12 weeks (data not shown). Thus, Akt activation in lung epithelium induces transient respiratory difficulties associated with lung maturational defects, which improves spontaneously after birth.

Akt activation in lung epithelial cells *in utero* results in increased numbers of CC10/SP-C double-positive cells and defective maturation of lung epithelial cells. In order to further assess the extent of epithelial differentiation, we performed Western bolt analysis of surfactant proteins (SP-A to SP-D) and immunohistochemistry of marker proteins: SP-C for type II alveolar epithelial cells, Clara cell 10-kDa protein (CC10) for Clara cells, aquaporin-5 (AQP5) for type I alveolar epithelial cells, and calcitonin gene-related peptide (CGRP) for neuroendocrine cells. Western blot analysis of surfactant proteins revealed downregulation of SP-B and upregulation of

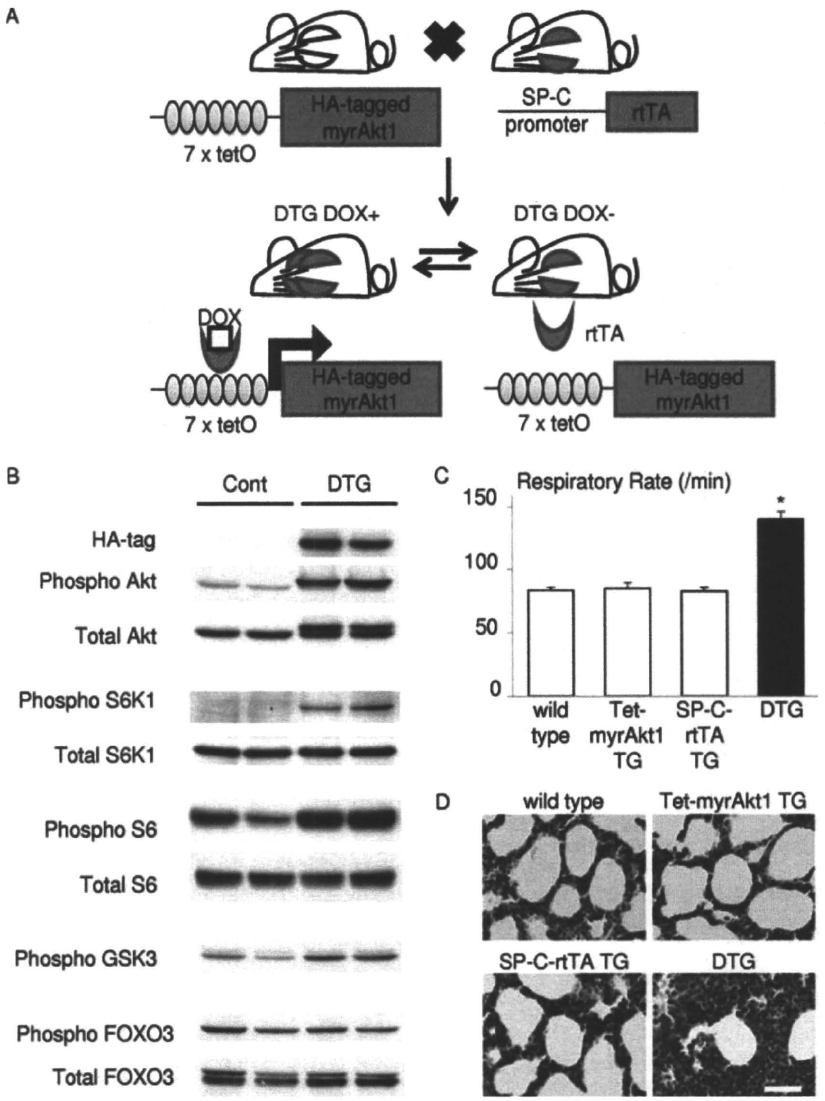

FIG. 1. Generation of bronchoalveolar epithelium-specific Akt1 TG mice. (A) Schematic illustration of binary TG system. (B) Western blot analysis of the whole-lung lysate from control and DTG mice at P0. (C) Respiratory rate at P0. DOX-treated SP-C-rtTA TG mice do not show respiratory distress. *, $P < 0.05$ versus DOX-treated wild-type, Tet-myrAkt1 TG mice, and SP-C-rtTA TG mice (n = 7, 5, 6, and 6 mice, respectively, from 3 dams). All animals were treated with DOX in the drinking water. (D) HE staining of the lung sections. Scale bar, 50 μm.

SP-D, whereas the expression levels of SP-A and SP-C were not altered (Fig. 3A). Western blot analysis and immunohistochemistry also revealed increased expression of CC10 and reduced expression of AQP5 in the lung of DTG mice (Fig. 3A and B). CGRP expression was not altered between control and DTG mice (date not shown). Previous studies characterized CC10/SP-C double-positive cells as BASCs that reside at the bronchoalveolar duct junction and differentiate to both Clara cells and type II alveolar epithelial cells; the latter further differentiate to type I alveolar epithelial cells (15). Double immunostaining revealed that CC10/SP-C double-positive cells were increased in number in the lung of DTG mice (Fig. 3C and D). Collectively, these findings suggest that aberrant activation of Akt signaling in lung epithelial cells results in increased numbers of CC10/SP-C double-positive cells and impaired differentiation of alveolar epithelial cells.

Akt activation in lung epithelial cells *in utero* results in RDS in preterm infants. Since RDS is more frequent in preterm infants than in full-term infants, we examined preterm infants born by Caesarean section at E18.5. DTG mice born at E18.5 showed cyanosis (Fig. 4A) associated with an irregular respiratory pattern, and all DTG mice died by 2 h after birth (Fig. 4B). The airway spaces of DTG lungs were filled with amorphous, proteinaceous material that was not observed in control lungs (Fig. 4C). PAS staining revealed that the size and the density of saccules in DTG lung were smaller and higher than those of controls, respectively (Fig. 4D to F). Western blot analysis of surfactant proteins revealed downregulation of SP-B, whereas the expression levels of SP-A, -C, and -D were not altered (Fig. 4G). Immunohistochemistry also revealed expansion of CC10/SP-C double-positive cells in the lung of DTG mice (Fig. 4H to J). AQP5 expression was barely detect-

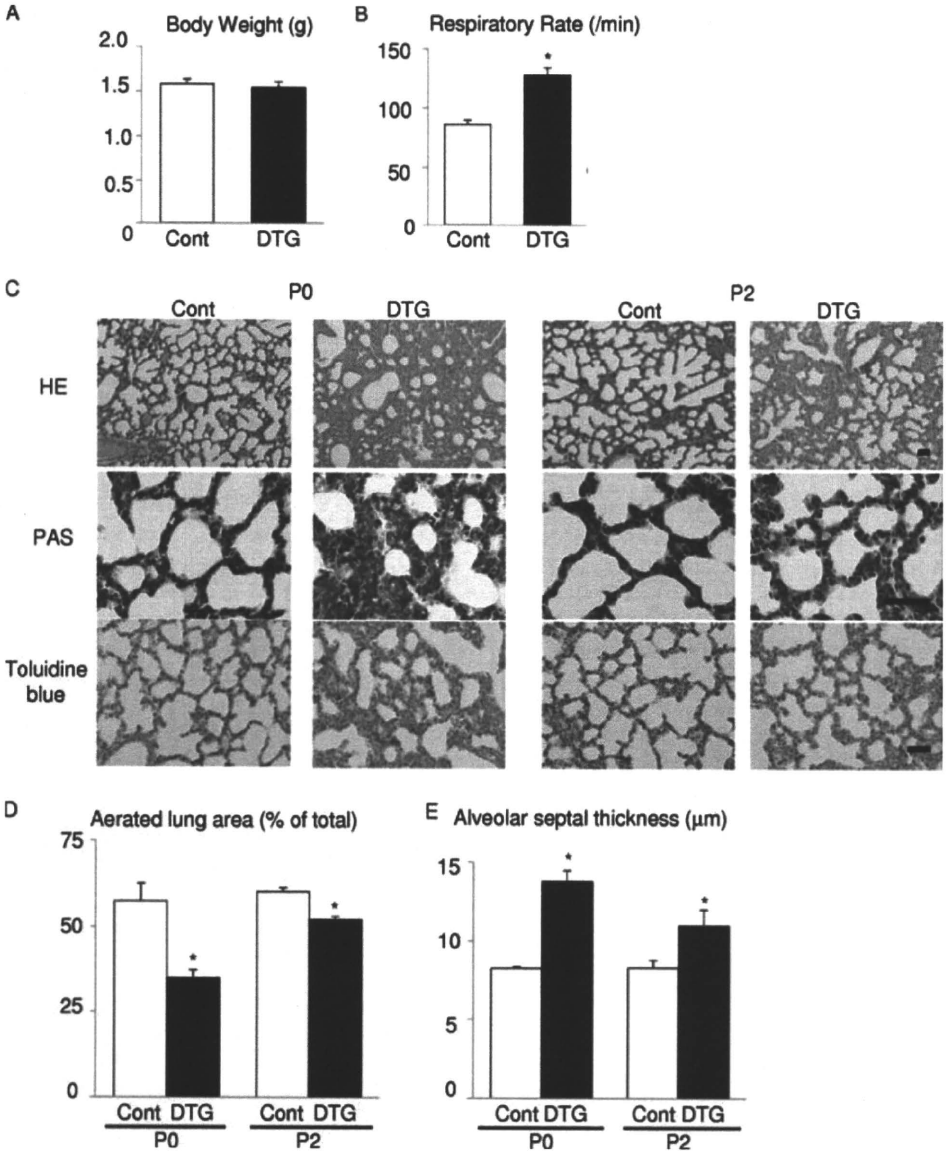

FIG. 2. Akt activation in lung epithelium induces tachypnea and delayed maturation of the lung. (A) Body weight at P0 of control (Cont; n = 6) and DTG (n = 4) mice from 2 dams. (B) Respiratory rate at P0 of control (n = 14) and DTG (n = 8) mice from 4 dams. (C) Histological analysis. HE, PAS, and toluidine blue staining of lung sections at P0 and P2. Scale bar, 50 mm. (D) Aerated lung area in control and DTG mice at P0 and P2. *, $P < 0.05$ versus control. (E) Thickness of alveolar septum in control and DTG mice at P0 and P2. *, $P < 0.05$ versus control. For experiments shown in panels D and E, n = 3 from a single dam under all conditions.

able at this stage (data not shown). These results collectively suggest that Akt activation in lung epithelial cells *in utero* results in RDS and perinatal lethality in preterm infants.

Rapamycin improves respiratory distress and lung maturational defects induced by Akt1 overexpression in lung epithelium. To test whether the Akt-mTOR pathway mediates lung pathology in DTG mice, rapamycin was administered to dams for 3 days (at E17.5, E18.5, and E19.5). Downregulation of mTOR signaling by rapamycin was confirmed by reduced phosphorylation levels of S6K1 (Fig. 5A). Examination of infants at P0 demonstrated that tachypnea observed in vehicle-treated DTG mice was improved by rapamycin treatment (Fig. 5B). Hematoxylin and eosin (HE) staining revealed that abnormal morphology of lung alveoli in DTG mice was reversed by rapamycin treatment (Fig. 5C, upper panel), and PAS staining demonstrated a reduced number of PAS-positive glycogen stores following rapamycin treatment (Fig. 5C, lower panel). By quantitative analysis of toluidine blue-stained sections, a decrease in aerated space and an increase in alveolar septal thickness observed in DTG mice were rescued by rapamycin treatment (Fig. 5D and E). Impaired differentiation of lung epithelial cells in DTG mice was also improved by rapamycin treatment, as evidenced by reduced expression of CC10, increased expression of AQP5, and a normal expression pattern of SP-C (Fig. 5F). These results suggest that mTOR is critically involved

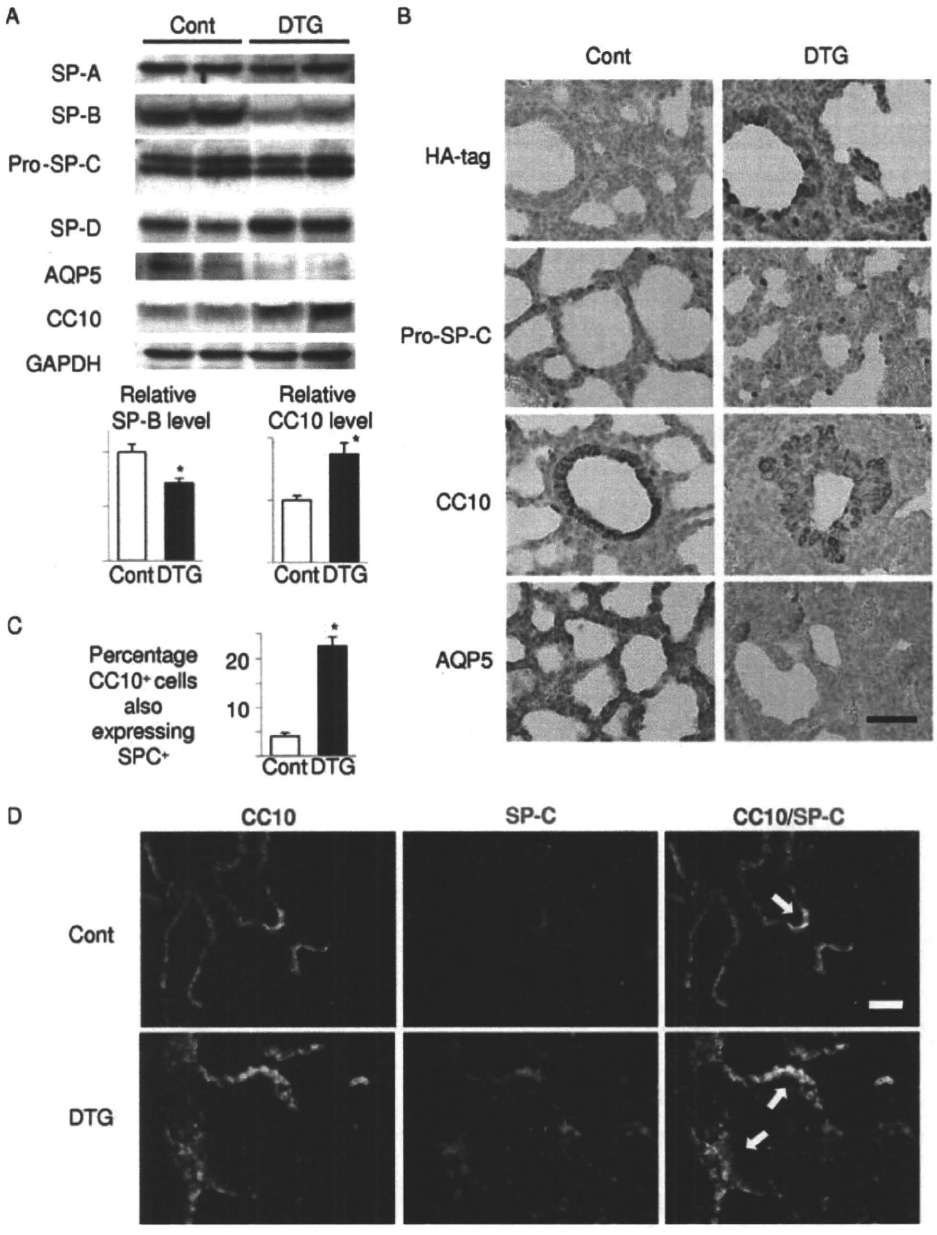

FIG. 3. Akt activation in lung epithelium results in defective maturation of lung epithelial cells and expansion of CC10/SP-C double-positive cells. (A) Western blot analysis of surfactant proteins (SP-A, SP-B, pro-SP-C, and SP-D), CC10 (a marker of Clara cells), and AQP5 (a marker of type I alveolar cells). Lower panels show densitometric analysis. *, $P < 0.05$ versus control ($n = 4$ mice from 2 dams for both controls and DTG). (B) Immunohistochemical analysis of HA tag (Akt1 transgene), SP-C, CC10, and AQP5. SP-C, CC10, and AQP5 were detected in cuboidal type II alveolar cells, Clara cells, and flat type I alveolar cells, respectively. Scale bar, 50 μm. (C and D). Double immunostaining of CC10 and SP-C. CC10/SP-C double-positive cells are indicated by arrows. Scale bar, 100 μm. *, $P < 0.05$ versus control ($n = 5$ control and $n = 3$ DTG mice from 3 dams).

in respiratory distress and lung maturational defects induced by Akt1 overexpression in lung epithelium.

Rapamycin improves respiratory distress induced by preterm delivery. The above-mentioned results suggest the possibility that mTOR activation mediates RDS in wild-type infants delivered preterm. To test this hypothesis, pregnant wild-type mice were treated with vehicle or rapamycin at E15.5 and E16.5, and pups were collected at E17.5 by Caesarean section. Inhibition of mTOR in the lung of rapamycin-treated pups was confirmed by reduced phosphorylation levels of S6K1 (Fig. 6A). All pups delivered from vehicle-treated dams died within 1 h after birth, whereas more than 50% of pups delivered from rapamycin-treated dams survived in this time frame (Fig. 6B). Histological examination revealed that rapamycin treatment promoted lung maturation, as demonstrated by increased aerated lung area, decreased alveolar septal wall thickness, a normal expression pattern of SP-C, and increased expression of AQP5 (Fig. 6C to F). Thus, downregulation of mTOR signal-

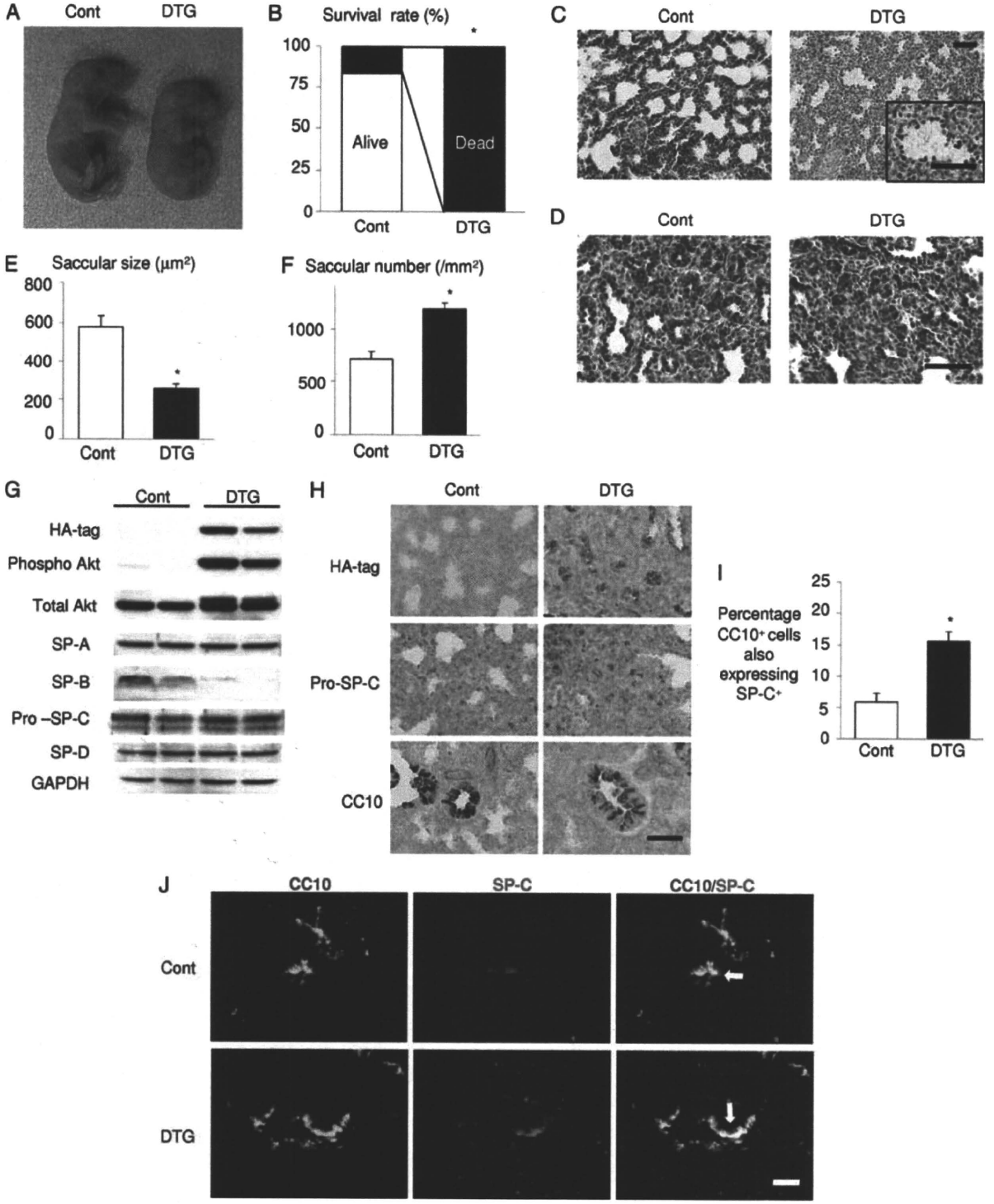

FIG. 4. Akt activation in lung epithelium results in RDS and lethality in preterm infants. (A) Gross appearance of infants. (B) Survival rate by 2 h after delivery. *, $P < 0.05$ ($n = 6$ control and $n = 5$ DTG mice from 2 dams). (C) HE staining of the lung sections of infants delivered by Caesarean section at E18.5. Scale bar, 50 μm. (D) PAS staining of the lung sections of infants delivered by Caesarean section at E18.5. Scale bar, 50 μm. (E) Saccular size at E18.5. *, $P < 0.05$ versus control. (F) Saccular number at E18.5. *, $P < 0.05$ versus control. For the experiments shown in panels E and F, $n = 3$ control and $n = 4$ DTG mice from 2 dams. (G) Western blot analysis of surfactant proteins (SP-A, SP-B, pro-SP-C, and SP-D). (H) Immunohistochemistry of HA tag (Akt1 transgene), pro-SP-C, and CC10 at E18.5. Scale bar, 50 μm. (I and J) Double immunostaining of CC10 and SP-C. CC10/SP-C double-positive cells are indicated by arrows. Scale bar, 100 μm. For both panels, $n = 4$ (Cont) and $n = 3$ (DTG) from 2 dams.

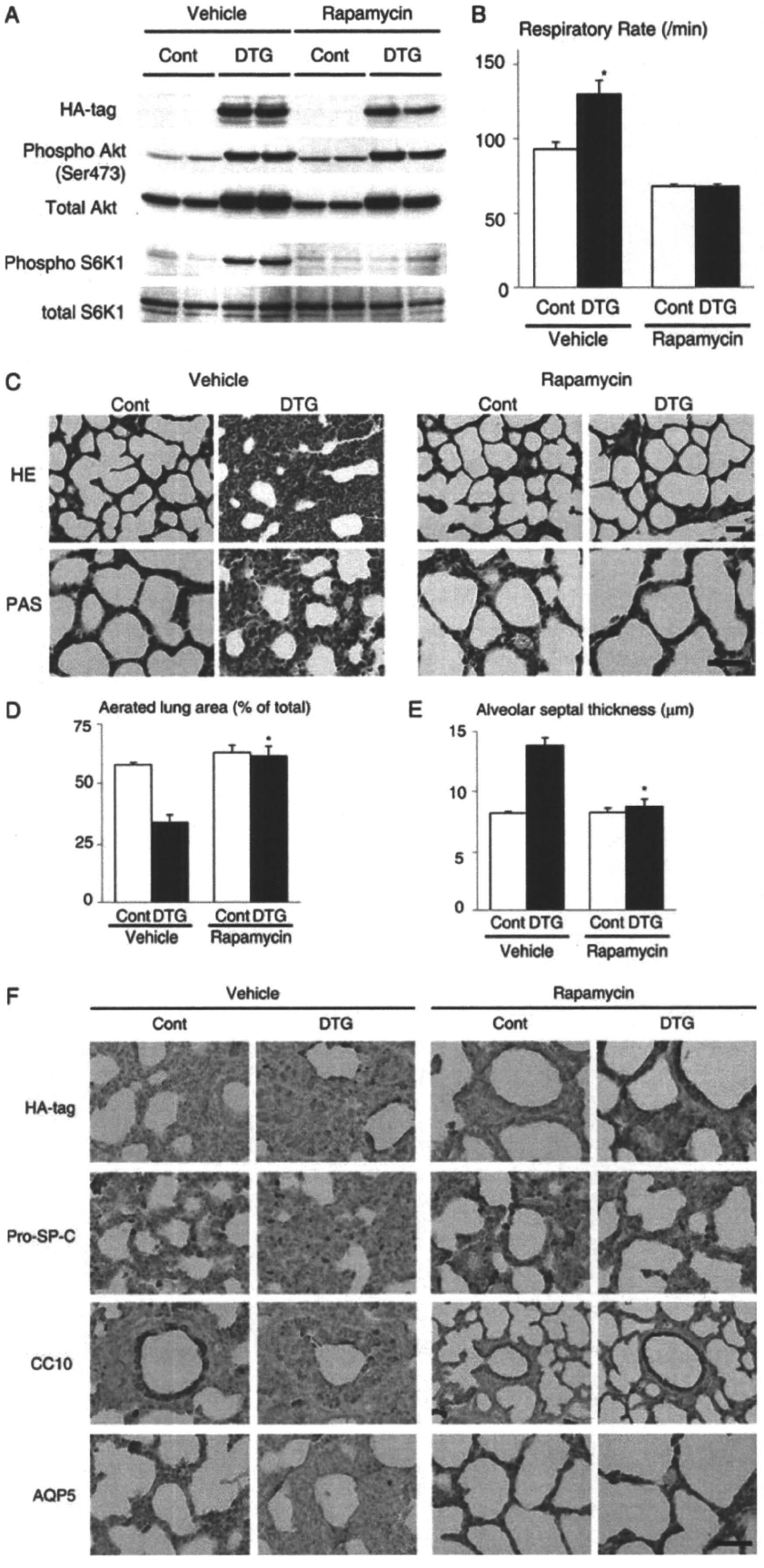
A
Vehicle
Rapamycin
Cont
DTG
Cont
DTG
HA-tag
Phospho Akt (Ser473)
Total Akt
Phospho S6K1
total S6K1
B
Respiratory Rate (/min)
150
100
50
0
Cont DTG
Cont DTG
Vehicle
Rapamycin
C
Vehicle
Rapamycin
Cont
DTG
Cont
DTG
HE
PAS
D
Aerated lung area (% of total)
75
50
25
0
Cont DTG
Cont DTG
Vehicle
Rapamycin
E
Alveolar septal thickness (μm)
15
10
5
0
Cont DTG
Cont DTG
Vehicle
Rapamycin
F
Vehicle
Rapamycin
Cont
DTG
Cont
DTG
HA-tag
Pro-SP-C
CC10
AQP5

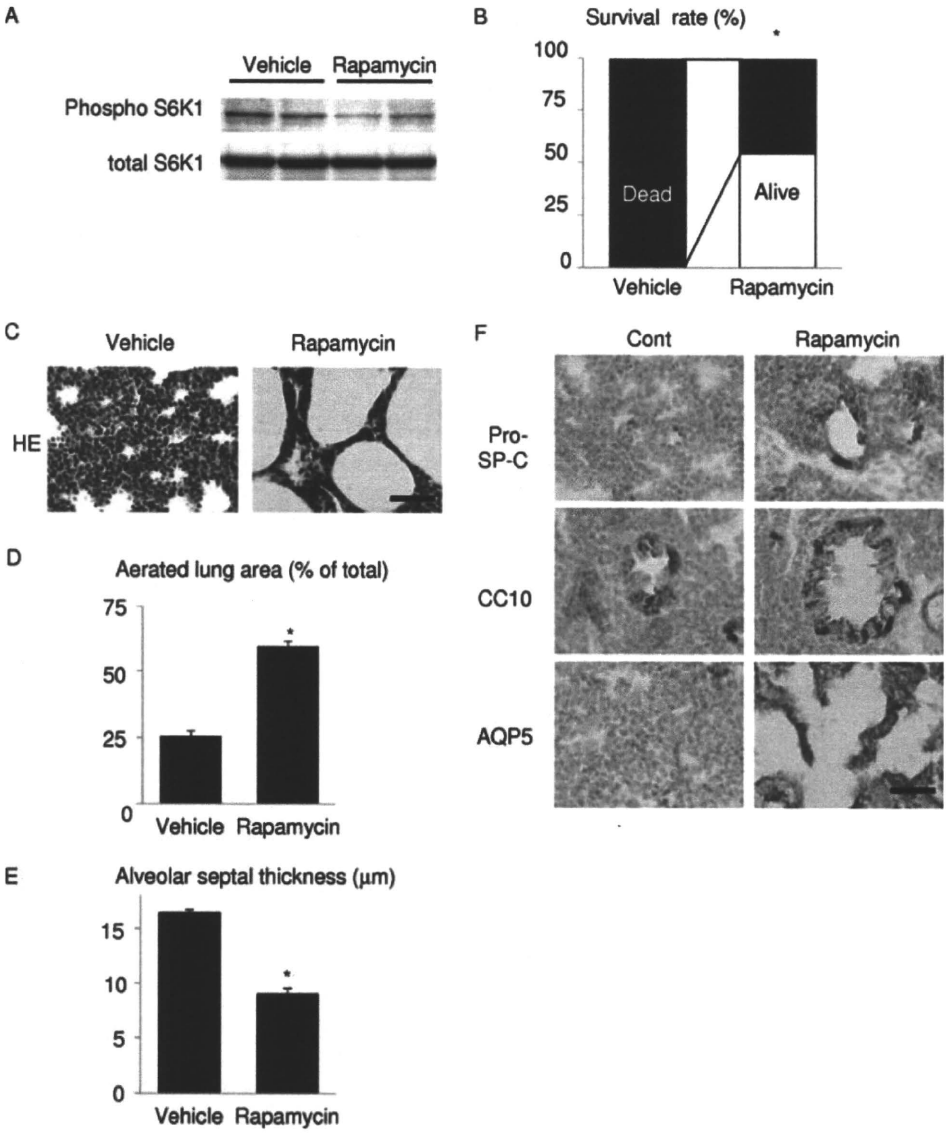

FIG. 6. Rapamycin improves respiratory distress and lung maturational defects induced by preterm delivery. (A) Western blot analysis of S6K1 in the lung. (B) Survival rate of wild-type pups 1 h after Caesarean section at E17.5. *, $P < 0.05$ versus vehicle-treated group. In the vehicle-treated group, $n = 15$ from a single dam. In the rapamycin group, $n = 24$ from 2 dams. (C) HE staining at 1 h after delivery. Scale bar, 50 μm. (D) Aerated lung area in vehicle- or rapamycin-treated pups. *, $P < 0.05$ versus vehicle-treated group. In the vehicle-treated group, $n = 3$ from a single dam; in the rapamycin group, $n = 4$ from 2 dams. (E) Thickness of alveolar septum in vehicle- or rapamycin-treated pups. *, $P < 0.05$ versus vehicle-treated group. In the vehicle-treated group, $n = 3$ from a single dam; in the rapamycin group, $n = 4$ from 2 dams. (F) Immunohistochemistry of pro-SP-C, CC10, and AQP5. Scale bar, 50 μm.

ing has a therapeutic potential for RDS induced by preterm delivery in wild-type mice.

Activation of the Akt-mTOR pathway attenuates HIF-2-dependent VEGF expression in lung epithelial cells. To investigate the mechanism by which Akt-mTOR signaling affects lung maturation, we examined the expression of VEGF, an angiogenic growth factor that is produced in the distal airway during late gestation and regulates coordinated development of alve-

FIG. 5. Rapamycin improves respiratory distress and lung maturational defects induced by Akt1 overexpression in lung epithelium. (A) Western blot analysis of Akt and S6K1 in the lung. (B) Respiratory rate of vehicle- or rapamycin-treated pups at P0. For vehicle experiments, $n = 7$ for both control and DTG mice from 3 dams; for rapamycin experiments, $n = 14$ (control) and $n = 11$ (DTG) mice from 4 dams. (C) Histological analysis. HE and PAS staining of lung sections at P0. Scale bar, 50 μm. (D) Aerated lung area in vehicle- or rapamycin-treated pups at P0. *, $P < 0.05$ versus vehicle-treated DTG mice. (E) Thickness of alveolar septum in vehicle- or rapamycin-treated pups at P0. *, $P < 0.05$ versus vehicle-treated DTG mice. For experiments shown in panels D and E, $n = 3$ control and $n = 3$ DTG vehicle-treated mice from 3 dams, and $n = 8$ control and $n = 7$ DTG rapamycin-treated mice from 4 dams. (F) Immunohistochemistry of HA tag, pro-SP-C, CC10, and AQP5 at P0. Scale bar, 50 μm.

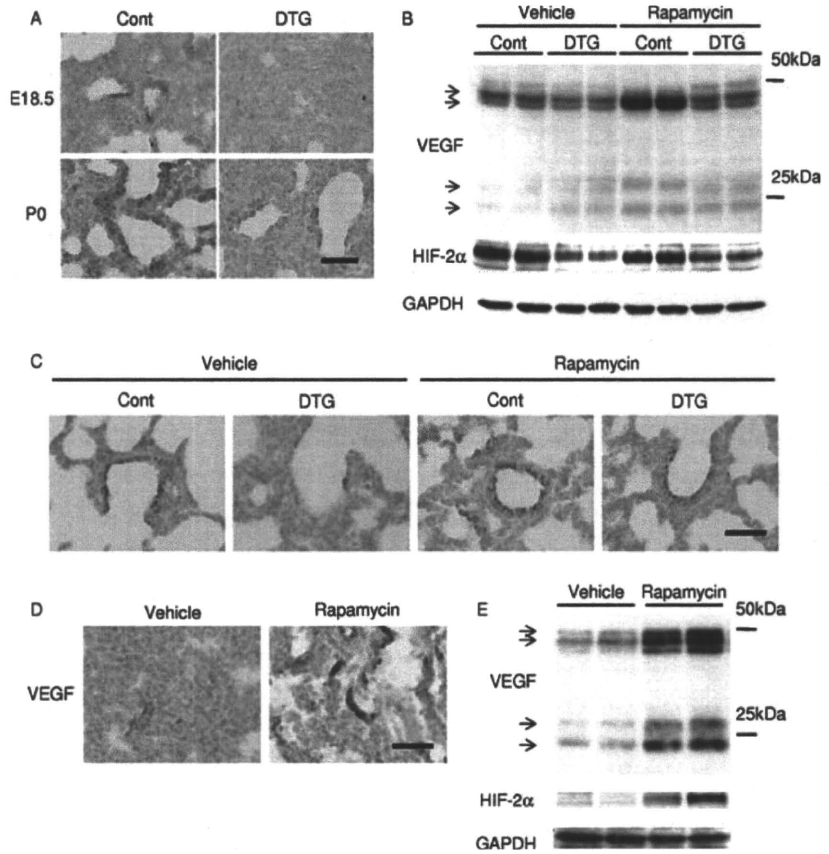

FIG. 7. Akt-mTOR pathway downregulates VEGF expression in the lung. (A) Immunostaining of VEGF at E18.5 and P0 in Akt1 TG mice. Scale bar, 50 μm. (B) Western blot analysis of VEGF and HIF-2α at P0 in Akt1 TG mice. (C) Immunostaining of VEGF at P0 in Akt1 TG mice. Scale bar, 50 μm. (D) Immunostaining of VEGF at E17.5 in wild-type mice. Scale bar, 50 μm. (E) Western blot analysis of VEGF and HIF-2α at E17.5 in wild-type mice.

olar epithelium and capillaries (4). Immunohistochemistry and Western blot analysis revealed that the expression levels of VEGF were downregulated in DTG mice both at E18.5 and P0 and were restored by rapamycin treatment (Fig. 7A to C). Since the expression of VEGF in the lung has been reported to depend on HIF-2 activity (4), we next examined the expression of HIF-2α protein in the lung. Western blot analysis revealed that the HIF-2α protein amount was downregulated in the lung of DTG mice (Fig. 7B). The expression levels of VEGF and HIF-2α were also examined in vehicle- or rapamycin-treated wild-type pups delivered at E17.5. Immunohistochemistry and Western blot analysis demonstrated the upregulation of VEGF and HIF-2α expression by rapamycin in wild-type mice delivered preterm (Fig. 7D and E). It was therefore concluded that activation of the Akt-mTOR pathway attenuates the expressions of VEGF and HIF-2α in the lung. However, it was also noted that the expression levels of HIF-2α do not necessarily correlate with those of VEGF because rapamycin treatment highly upregulated VEGF expression in control animals without altering HIF-2α expression levels (Fig. 7B, compare the vehicle control group and the rapamycin control group). We therefore examined whether Akt-mTOR signaling regulates the transcriptional activity of HIF-2. In cultured A549 lung epithelial cells, insulin induced downregulation of VEGF expression, which was reversed by rapamycin treatment (Fig. 8A). Luciferase assays using *VEGF-luc* as a reporter gene revealed that insulin attenuated transcriptional activity of HIF-2 on VEGF promoter, which was reversed by rapamycin treatment (Fig. 8B), while both insulin and rapamycin had minimal effects on HIF-1 transcriptional activity (Fig. 8C). These results suggest that activation of Akt-mTOR signaling attenuates HIF-2-dependent VEGF expression with respect to both the amount of HIF-2α protein and HIF-2 transcriptional activity.

Activation of the Akt-mTOR pathway reduces alveolar capillary density. To test whether Akt-mTOR-mediated downregulation of VEGF is associated with attenuated alveolar angiogenesis, vascular morphometry was performed in DTG and control mice at P0. Isolectin B4 staining revealed that alveolar capillary density was significantly reduced in DTG mice compared to that in control mice, and this reduction was rescued by rapamycin treatment (Fig. 9A and B). We also found that alveolar capillary density in wild-type mice delivered preterm at E17.5 was increased by rapamycin treatment (Fig. 9C and D). Thus, alveolar capillary density is closely linked to the level of VEGF expression in the lung. These results are consistent with our hypothesis that Akt-mTOR signaling promotes RDS through downregulation of VEGF.

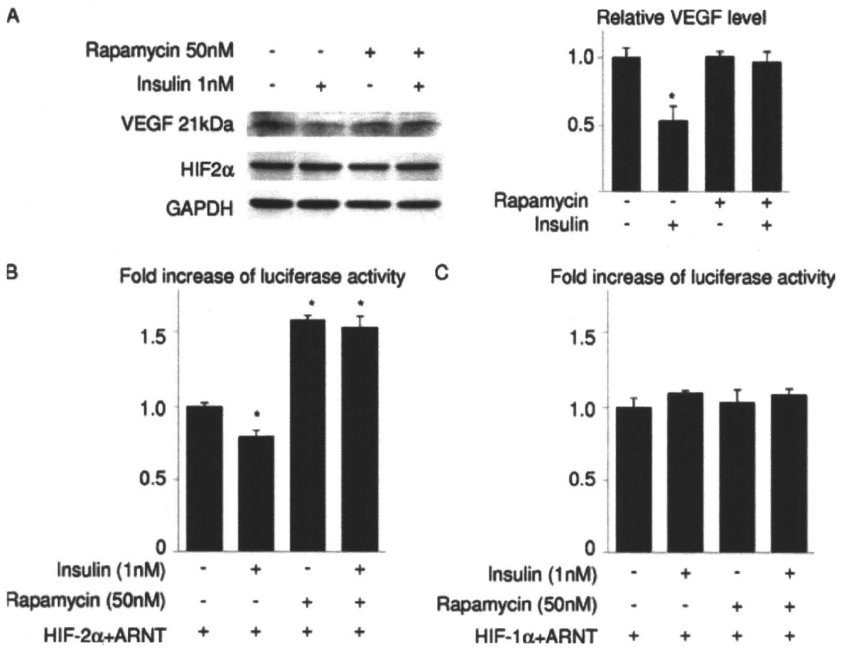

FIG. 8. Insulin attenuates VEGF expression and HIF-2 transcriptional activity on *VEGF* promoter in an mTOR-dependent manner in lung epithelial cells. (A) Western blot analysis of VEGF and HIF-2α in A549 cells treated with insulin and/or rapamycin for 48 h. The right panel shows the densitometric analysis. *, $P < 0.05$ versus the rapamycin (−)/insulin (−) group ($n = 3$ for each group). (B and C) Luciferase assays in A549 cells. A549 cells were transfected with a *VEGF-luc* reporter and expression vectors for HIF-1α, HIF-2α, and ARNT and treated with insulin and/or rapamycin. All experiments were performed in the presence of $CoCl_2$ to mimic hypoxic conditions. *, $P < 0.05$ versus the rapamycin (−)/insulin (−) group.

DISCUSSION

In this study we have demonstrated that activation of Akt signaling in lung epithelial cells during embryogenesis results in transient respiratory difficulties in full-term infants and in RDS in preterm infants. These respiratory defects were associated with bronchiolar hyperplasia, expansion of CC10/SP-C double-positive cells, and impaired maturation of lung epithelial cells. We also found that Akt-mTOR signaling is critically involved in the pathogenesis of RDS because rapamycin treatment improved respiratory distress and lung maturational defects induced by Akt activation or preterm delivery. Mechanistically, Akt-mTOR signaling attenuates both the protein amounts and transcriptional activity of HIF-2, leading to downregulation of HIF-2-dependent expression of VEGF, an angiogenic growth factor that is required for maturation of alveolar epithelial cells. These observations suggest the possibility that aberrant activation of Akt-mTOR signaling or preterm delivery before the appropriate downregulation of this signaling axis plays a causal role in RDS through downregulation of HIF-2-dependent VEGF expression and that the mTOR-HIF-2 pathway may be a novel therapeutic target for infant RDS.

RDS is frequently observed in infants of diabetic mothers, and hyperactivation of insulin signaling in response to maternal hyperglycemia has been proposed to play a pathogenic role (19, 22). It was also previously shown that alveolar epithelium-specific deletion of *Pten* results in RDS, with approximately 90% of neonates dying within 2 h after birth (33). This phenotype of conditional *Pten* deletion is more severe than that of alveolar epithelium-specific Akt1 transgenic mice, suggesting the possibility that PI3K-dependent but Akt-independent pathways are also implicated in the occurrence of RDS. However, because another line of lung epithelium-specific *Pten* knockout mice generated by a similar method exhibit a very mild phenotype (i.e., lack of neonatal lethality, normal postnatal development, and mild bronchiolar hyperplasia) (7), the variation of phenotypes among different animal models may be due in part to the differences in the genetic background of the animals. Furthermore, rapamycin treatment of dams significantly improved the phenotype of alveolar epithelium-specific Akt1 transgenic mice. Taken together, these observations suggest that activation of the PI3K-Akt-mTOR pathway in lung epithelial cells *in utero* plays a causal role in the pathogenesis of RDS in infants with diabetic mothers.

Lung development in mice is histologically divided into four phases: the pseudoglandular stage (E9.5 to 16.5), canalicular stage (E16.5 to 17.5), terminal sac stage (E17.5 to P5), and alveolar stage (P5 to P30) (30). Differentiation of type I and type II epithelial cells and high levels of Pten expression in respiratory epithelium occur at the terminal sac stage (17), which is consistent with the idea that downregulation of the PI3K-Akt-mTOR pathway is required for epithelial differentiation. In humans, lung development is relatively advanced compared with that of mice, and the terminal sac stage corresponds to human preterm infants between 26 and 36 weeks of gestation, when a high complication rate of RDS is observed. Thus, inhibition of the PI3K-Akt-mTOR pathway at specific time points during a later stage of embryogenesis appears to be critical for normal lung development and maturation, and aberrant activation of Akt-mTOR signaling or preterm delivery

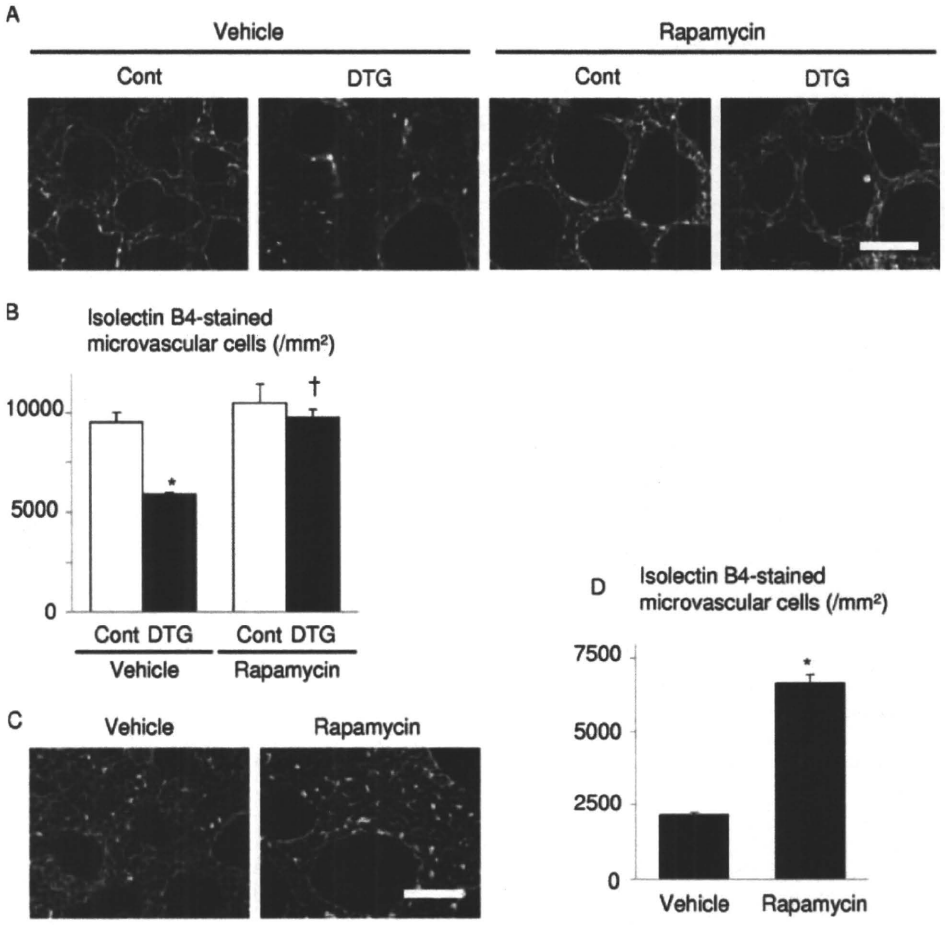

FIG. 9. Alveolar capillary bed formation is impaired by Akt1 overexpression in lung epithelium, which is improved by rapamycin administration to the dams. (A) Histological analysis of vehicle- or rapamycin-treated pups at P0. Sections were stained with isolectin B4-FITC conjugate (green) to detect endothelial cells and with wheat germ agglutinin-TRITC conjugate (red) for membrane staining. Scale bar, 50 μm. (B) Alveolar capillary density. *, $P < 0.05$ versus vehicle-treated control mice; †, $P < 0.05$ versus vehicle-treated DTG mice. In the vehicle-treated group, $n = 4$ control and $n = 3$ DTG mice from 2 dams; in the rapamycin group, $n = 4$ control and $n = 4$ DTG mice from 2 dams. (C) Histological analysis of vehicle- or rapamycin-treated wild-type pups born by Caesarean section at E17.5. Scale bar, 50 μm. (D) Alveolar capillary density. *, $P < 0.05$ versus vehicle-treated mice ($n = 4$ vehicle-treated mice from a single dam, and $n = 4$ rapamycin-treated mice from 2 dams).

before this signaling pathway is appropriately downregulated may result in the occurrence of RDS. The observation that rapamycin was effective for RDS also suggests that downregulation of mTOR signaling is sufficient to induce maturation of lung epithelial cells. Previous studies also implicated GATA6-Wnt/β-catenin signaling and calcineurin/nuclear factor of activated T cells (NFAT) signaling in lung maturation (6, 34). How these two signaling pathways and the PI3K-Akt-mTOR pathway coordinately regulate normal lung development remains to be investigated. It should also be noted that VEGF-induced angiogenesis is enhanced in the presence of rapamycin, which is inconsistent with the observation that VEGF induces endothelial cell proliferation via the Akt-mTOR pathway (32). This may be in part explained by the proangiogenic effects of the rapamycin-insensitive downstream effectors of Akt such as glycogen synthase kinase-3 and the FOXO family of transcription factors (1, 16).

Epithelial-endothelial interactions during lung development are critical in establishing a functional blood-gas interface, and normal lung function depends on the coordinated development of alveolar epithelium and capillaries, which is primarily regulated by VEGF (27). It was previously shown that deletion of HIF-2α in mice causes RDS due to downregulation of HIF-2-dependent VEGF expression in the lung (4). The similarity of the phenotypes between lung epithelium-specific Akt1 TG mice and HIF-2α-deficient mice prompted us to investigate the mechanistic link between mTOR and HIF-2. Previous studies showed that mTOR enhances the transcriptional activity of HIF-1 (13) and that VEGF expression in the heart is induced by activation of the Akt-mTOR pathway in TG mice in which the Akt1 transgene is inducible in the heart by doxycycline treatment (25), suggesting that mTOR promotes HIF-1-dependent VEGF expression. However, VEGF expression in the lung was downregulated by Akt1 overexpression and restored by rapamycin treatment. Consistently, HIF-2α expression levels were downregulated in the lung of DTG mice, and reporter gene assays in cultured lung epithelial cells revealed that insulin attenuates the transcriptional activity of HIF-2 on VEGF promoter in an mTOR-dependent manner. These results suggest the possibility that HIF-2 and VEGF are situated down-

stream of mTOR in the pathogenesis of RDS and that activation of the Akt-mTOR pathway in the lung leads to RDS through the downregulation of HIF-2-dependent VEGF expression. How mTOR differentially regulates the transcriptional activity of HIF-1 and HIF-2 awaits further investigation.

There are several limitations in this study. First, because the experiments to test whether overexpression of HIF-2 or VEGF in lung epithelium rescues the RDS phenotype of Akt1 TG mice were not performed, the direct link between the Akt-mTOR pathway and the HIF-2-VEGF pathway remains to be determined. Second, although it is highly possible that hyperactivation of insulin signaling plays a causal role in RDS (8, 10, 11), the present study does not provide definitive evidence showing that insulin signaling is, indeed, activated in lung epithelium of infants having a diabetic mother. It is also possible that other factors that activate the PI3K-Akt-mTOR pathway (e.g., insulin-like growth factors) may be involved in the pathogenesis of RDS. Third, the TG mouse system used in this study may activate Akt in the lung to a supra-physiological level that is not comparable to the level of Akt activation observed in infants of diabetic mothers.

In summary, the present study demonstrates a crucial role for the Akt-mTOR pathway in the pathogenesis of infant RDS and suggests that the mTOR-HIF-2 signaling axis is a novel therapeutic target for this disease state.

ACKNOWLEDGMENTS

We thank S. L. McKnight for phEP-1, A. Ochiai and G. Ishii for A549 cells, and E. Fujita, R. Kobayashi, and Y. Ishiyama for technical assistance.

This work was supported by grants from the Ministry of Education, Culture, Sports, Science and Technology to I.K.

We declare that we have no conflicts of interest.

REFERENCES

1. **Abid, M. R., et al.** 2004. Vascular endothelial growth factor activates PI3K/Akt/forkhead signaling in endothelial cells. Arterioscler. Thromb. Vasc. Biol. **24:**294–300.
2. **Bentley-Lewis, R., S. Levkoff, A. Stuebe, and E. W. Seely.** 2008. Gestational diabetes mellitus: postpartum opportunities for the diagnosis and prevention of type 2 diabetes mellitus. Nat. Clin. Pract. Endocrinol. Metab. **4:**552–558.
3. **Clausen, T. D., et al.** 2005. Poor pregnancy outcome in women with type 2 diabetes. Diabetes Care **28:**323–328.
4. **Compernolle, V., et al.** 2002. Loss of HIF-2α and inhibition of VEGF impair fetal lung maturation, whereas treatment with VEGF prevents fatal respiratory distress in premature mice. Nat. Med. **8:**702–710.
5. **Crowther, C. A., et al.** 2005. Effect of treatment of gestational diabetes mellitus on pregnancy outcomes. N. Engl. J. Med. **352:**2477–2486.
6. **Dave, V., et al.** 2006. Calcineurin/Nfat signaling is required for perinatal lung maturation and function. J. Clin. Invest. **116:**2597–2609.
7. **Dave, V., et al.** 2008. Conditional deletion of Pten causes bronchiolar hyperplasia. Am. J. Respir. Cell Mol. Biol. **38:**337–345.
8. **Dekowski, S. A., and J. M. Snyder.** 1992. Insulin regulation of messenger ribonucleic acid for the surfactant-associated proteins in human fetal lung in vitro. Endocrinology **131:**669–676.
9. **Feig, D. S., and V. A. Palda.** 2002. Type 2 diabetes in pregnancy: a growing concern. Lancet **359:**1690–1692.
10. **Guttentag, S. H., D. S. Phelps, W. Stenzel, J. B. Warshaw, and J. Floros.** 1992. Surfactant protein A expression is delayed in fetuses of streptozotocin-treated rats. Am. J. Physiol. **262:**L489–L494.
11. **Guttentag, S. H., D. S. Phelps, J. B. Warshaw, and J. Floros.** 1992. Delayed hydrophobic surfactant protein (SP-B, SP-C) expression in fetuses of streptozotocin-treated rats. Am. J. Respir. Cell Mol. Biol. **7:**190–197.
12. **Hallman, M., V. Glumoff, and M. Ramet.** 2001. Surfactant in respiratory distress syndrome and lung injury. Comp. Biochem. Physiol. Part A **129:**287–294.
13. **Hudson, C. C., et al.** 2002. Regulation of hypoxia-inducible factor 1α expression and function by the mammalian target of rapamycin. Mol. Cell. Biol. **22:**7004–7014.
14. **Jensen, D. M., et al.** 2004. Outcomes in type 1 diabetic pregnancies: a nationwide, population-based study. Diabetes Care **27:**2819–2823.
15. **Kim, C. F., et al.** 2005. Identification of bronchioalveolar stem cells in normal lung and lung cancer. Cell **121:**823–835.
16. **Kim, H. S., et al.** 2002. Regulation of angiogenesis by glycogen synthase kinase-3β. J. Biol. Chem. **277:**41888–41896.
17. **Luukko, K., A. Ylikorkala, M. Tiainen, and T. P. Makela.** 1999. Expression of LKB1 and PTEN tumor suppressor genes during mouse embryonic development. Mech. Dev. **83:**187–190.
18. **Maemura, K., et al.** 1999. Generation of a dominant-negative mutant of endothelial PAS domain protein 1 by deletion of a potent C-terminal transactivation domain. J. Biol. Chem. **274:**31565–31570.
19. **Montan, S., and S. Arulkumaran.** 2006. Neonatal respiratory distress syndrome. Lancet **367:**1878–1879.
20. **Morimoto, M., and R. Kopan.** 2009. rtTA toxicity limits the usefulness of the SP-C-rtTA transgenic mouse. Dev. Biol. **325:**171–178.
21. **Nold, J. L., and M. K. Georgieff.** 2004. Infants of diabetic mothers. Pediatr. Clin. North Am. **51:**619–637.
22. **Northway, W. H., Jr., R. C. Rosan, and D. Y. Porter.** 1967. Pulmonary disease following respirator therapy of hyaline-membrane disease. Bronchopulmonary dysplasia. N. Engl. J. Med. **276:**357–368.
23. **Perl, A. K., S. E. Wert, A. Nagy, C. G. Lobe, and J. A. Whitsett.** 2002. Early restriction of peripheral and proximal cell lineages during formation of the lung. Proc. Natl. Acad. Sci. U. S. A. **99:**10482–10487.
24. **Shioi, T., et al.** 2003. Rapamycin attenuates load-induced cardiac hypertrophy in mice. Circulation **107:**1664–1670.
25. **Shiojima, I., et al.** 2005. Disruption of coordinated cardiac hypertrophy and angiogenesis contributes to the transition to heart failure. J. Clin. Invest. **115:**2108–2118.
26. **Shiojima, I., et al.** 2002. Akt signaling mediates postnatal heart growth in response to insulin and nutritional status. J. Biol. Chem. **277:**37670–37677.
27. **Stenmark, K. R., and S. H. Abman.** 2005. Lung vascular development: implications for the pathogenesis of bronchopulmonary dysplasia. Annu. Rev. Physiol. **67:**623–661.
28. **Taniguchi, C. M., B. Emanuelli, and C. R. Kahn.** 2006. Critical nodes in signalling pathways: insights into insulin action. Nat. Rev. Mol. Cell Biol. **7:**85–96.
29. **Tichelaar, J. W., W. Lu, and J. A. Whitsett.** 2000. Conditional expression of fibroblast growth factor-7 in the developing and mature lung. J. Biol. Chem. **275:**11858–11864.
30. **Warburton, D., et al.** 2000. The molecular basis of lung morphogenesis. Mech. Dev. **92:**55–81.
31. **Whitsett, J. A., and T. E. Weaver.** 2002. Hydrophobic surfactant proteins in lung function and disease. N. Engl. J. Med. **347:**2141–2148.
32. **Xue, Q., et al.** 2009. Rapamycin inhibition of the Akt/mTOR pathway blocks select stages of VEGF-A164-driven angiogenesis, in part by blocking S6Kinase. Arterioscler. Thromb. Vasc. Biol. **29:**1172–1178.
33. **Yanagi, S., et al.** 2007. Pten controls lung morphogenesis, bronchioalveolar stem cells, and onset of lung adenocarcinomas in mice. J. Clin. Invest. **117:**2929–2940.
34. **Zhang, Y., et al.** 2008. A Gata6-Wnt pathway required for epithelial stem cell development and airway regeneration. Nat. Genet. **40:**862–870.

Docking Protein Gab1 Is an Essential Component of Postnatal Angiogenesis After Ischemia via HGF/c-Met Signaling

Wataru Shioyama, Yoshikazu Nakaoka, Kaori Higuchi, Takashi Minami, Yoshiaki Taniyama, Keigo Nishida, Hiroyasu Kidoya, Takashi Sonobe, Hisamichi Naito, Yoh Arita, Takahiro Hashimoto, Tadashi Kuroda, Yasushi Fujio, Mikiyasu Shirai, Nobuyuki Takakura, Ryuichi Morishita, Keiko Yamauchi-Takihara, Tatsuhiko Kodama, Toshio Hirano, Naoki Mochizuki, Issei Komuro

Rationale: **Grb2-associated binder (Gab) docking proteins, consisting of Gab1, Gab2, and Gab3, have crucial roles in growth factor–dependent signaling. Various proangiogenic growth factors regulate angiogenesis and endothelial function. However, the roles of Gab proteins in angiogenesis remain elusive.**

Objective: **To elucidate the role of Gab proteins in postnatal angiogenesis.**

Methods and Results: **Endothelium-specific Gab1 knockout (Gab1ECKO) mice were viable and showed no obvious defects in vascular development. Therefore, we analyzed a hindlimb ischemia (HLI) model of control, Gab1ECKO, or conventional Gab2 knockout (Gab2KO) mice. Intriguingly, impaired blood flow recovery and necrosis in the operated limb was observed in all of Gab1ECKO, but not in control or Gab2KO mice. Among several proangiogenic growth factors, hepatocyte growth factor (HGF) induced the most prominent tyrosine phosphorylation of Gab1 and subsequent complex formation of Gab1 with SHP2 (Src homology-2–containing protein tyrosine phosphatase 2) and phosphatidylinositol 3-kinase subunit p85 in human endothelial cells (ECs). Gab1-SHP2 complex was required for HGF-induced migration and proliferation of ECs via extracellular signal-regulated kinase (ERK)1/2 pathway and for HGF-induced stabilization of ECs via ERK5. In contrast, Gab1-p85 complex regulated activation of AKT and contributed partially to migration of ECs after HGF stimulation. Microarray analysis demonstrated that HGF upregulated angiogenesis-related genes such as *KLF2* (Krüppel-like factor 2) and *Egr1* (early growth response 1) via Gab1-SHP2 complex in human ECs. In Gab1ECKO mice, gene transfer of vascular endothelial growth factor, but not HGF, improved blood flow recovery and ameliorated limb necrosis after HLI.**

Conclusion: **Gab1 is essential for postnatal angiogenesis after ischemia via HGF/c-Met signaling. (*Circ Res*. 2011; 108:664-675.)**

Key Words: angiogenesis ■ Gab1 ■ growth factors ■ endothelial cells ■ signal transduction

The Grb2-associated binder (Gab) family docking proteins, consisting of Gab1, Gab2, and Gab3, are involved in amplification and integration of signal transduction evoked by growth factors, cytokines, antigens, and numerous other molecules.[1,2] Gab proteins lack enzymatic activity but become phosphorylated on tyrosine residues, providing binding sites for multiple Src homology-2 (SH2) domain-containing proteins such as SH2 containing protein tyrosine phosphatase 2 (SHP2), phosphatidylinositol 3-kinase regulatory subunit p85, phospholipase Cγ, Crk, and GC-GAP. Docking of Gab proteins to SHP2 and p85 is considered to be essential for activation of mitogen activated protein kinase (MAPK), such as extracellular signal-regulated kinase (ERK)1/2 and AKT, respectively.[1,2] Conventional Gab1 knockout (Gab1KO) mice

Original received September 8, 2010; revision received January 20, 2011; accepted January 24, 2011. In December 2010, the average time from submission to first decision for all original research papers submitted to *Circulation Research* was 14.5 days.

From the Departments of Cardiovascular Medicine (W.S., Y.N., K.H., Y.A., T. Hashimoto, T. Kuroda, K.Y.-T., I.K.), Clinical Gene Therapy (Y.T., R.M.), and Advanced Cardiovascular Therapeutics (T. Kuroda), Osaka University Graduate School of Medicine, Suita; Research Center for Advanced Science and Technology (T.M., T. Kodama), University of Tokyo, Laboratory for System Biology and Medicine; Laboratory for Cytokine Signaling (K.N., T. Hirano), RIKEN Research Center for Allergy and Immunology, Yokohama; Department of Signal Transduction (H.K., H.N., N.T.), Research Institute for Microbial Diseases, Osaka University, Suita; Departments of Cardiac Physiology (T.S., M.S.) and Cell Biology (N.M.), National Cerebral and Cardiovascular Center Research Institute, Suita; Department of Clinical Pharmacology and Pharmacogenomics (Y.F.), Osaka University Graduate School of Pharmaceutical Sciences, Suita; and Laboratory of Developmental Immunology (T. Hirano), JST-CREST, Graduate School of Frontier Biosciences and Graduate School of Medicine, and WPI Immunology Frontier Research Center, Osaka University, Suita, Japan.

This manuscript was sent to Kathy Griendling, Consulting Editor, for review by expert referees, editorial decision, and final disposition.

Correspondence to Issei Komuro, MD, PhD, or Yoshikazu Nakaoka, MD, PhD, Department of Cardiovascular Medicine, Osaka University Graduate School of Medicine, 2-2, Yamadaoka, Suita, Osaka, 565-0871, Japan. E-mail komuro-tky@umin.ac.jp or ynakaoka@imed3.med.osaka-u.ac.jp

Circulation Research **is available at http://circres.ahajournals.org** **DOI: 10.1161/CIRCRESAHA.110.232223**

display embryonic lethality with impaired development of heart, placenta, skin, and skeletal muscle.[3,4] Conventional Gab2 knockout (Gab2KO) mice do not show any obvious developmental defects, but display impaired allergic responses, osteoclast defects, and abnormal hematopoiesis in adulthood.[5–7] Gab3 knockout mice exhibit no obvious phenotype.[8] Because Gab1KO mice are embryonic lethal, we and others created conditional knockout mice of Gab1 using the *Cre-loxP* system.[9–12] We created cardiomyocyte-specific Gab1/Gab2 double knockout mice and reported that Gab1 and Gab2 have the redundant roles for maintenance of cardiac function via neuregulin-1/ErbB signaling.[11]

Angiogenesis, the process of new blood vessel formation, is involved in many physiological and pathological settings such as ischemia, atherosclerosis, diabetes, and cancer.[13] During angiogenic growth, some endothelial cells (ECs) within capillary vessel wall are selected for "sprouting" and acquire invasive and motile behaviors. The tip cells, which lead the growing sprout, are guided by vascular endothelial growth factor (VEGF) gradients. The migration and proliferation of ECs behind the tip promote sprout extension. Fusion processes at the EC-EC interfaces establish a continuous lumen and blood flow promote maturation processes such as the "stabilization" of cell junctions and tight pericyte recruitment.[14,15] The angiogenic growth consists of these multistep processes from "endothelial sprouting" to "endothelial stabilization." ERK5 has been reported to have a central role for flow-mediated stabilization via upregulation of endothelial stabilization factor Krüppel-like factor (KLF)2.[16,17] However, the molecular mechanism how ERK5-KLF2 pathway is activated in in vivo angiogenesis remains unclear to date.

We reported an important role of Gab1 for ERK5 activation in gp130-dependent cardiomyocyte hypertrophy.[18,19] On the other hand, it has been reported that Gab1 has a role for VEGF-dependent signaling in the in vitro experiments using ECs.[20–22] However, the in vivo role of Gab proteins in angiogenesis has not been addressed to date. Here, we demonstrate that Gab1 in the vascular endothelium is essential for postnatal angiogenesis after ischemia. Endothelium-specific deletion of Gab1 results in enhanced propensity to limb necrosis after hindlimb ischemia (HLI) caused by impaired angiogenesis via hepatocyte growth factor (HGF)/c-Met signaling. On the contrary, global deletion of Gab2, another Gab protein expressed in the vascular endothelium, does not lead to limb necrosis and impairment of blood flow recovery after HLI compared with control mice. Consistently, Gab1, but not Gab2, is required for activation of ERK1/2, ERK5, and AKT after stimulation with HGF in ECs. Gab1 associates with SHP2 and p85 after stimulation with HGF in ECs. Gab1-SHP2 complex positively regulates migration and proliferation of ECs via ERK1/2 and contributes to stabilization of ECs via ERK5 presumably in association with upregulation of KLF2.

Methods

An expanded Methods section is available in the Online Data Supplement at http://circres.ahajournals.org.

Non-standard Abbreviations and Acronyms

β-gal	β-galactosidase
CA	constitutively active
DN	dominant-negative
EC	endothelial cell
Egr	early growth response
ERK	extracellular signal-regulated kinase
FGF	fibroblast growth factor
Gab	Grb2-associated binder
Gab1ECKO	endothelium-specific Gab1 knockout
Gab1KO	conventional Gab1 knockout
Gab2KO	conventional Gab2 knockout
GST	glutathione *S*-transferase
HGF	hepatocyte growth factor
HLI	hindlimb ischemia
HUVEC	human umbilical vein endothelial cell
KLF	Krüppel-like factor
LDBF	laser Doppler blood flow
MACS	Magnetic Cell Sorting
MAPK	mitogen activated protein kinase
MEF2C	myocyte enhancer factor 2
MEK	mitogen activated protein kinase/extracellular signal-regulated kinase
SHP2	Src homology-2–containing protein tyrosine phosphatase 2
siRNA	small interfering RNA
TM	thrombomodulin
VEGF	vascular endothelial growth factor

Animals

Gab1^{flox} mice were generated in 129/Sv-C57BL/6J mixed background as described previously.[11] *Tie2-Cre* transgenic mice in CD-1 background were provided from Dr Thomas N. Sato.[23] Endothelium-specific Gab 1 knockout (Gab1ECKO) mice were generated by crossing *Gab1*$^{flox/flox}$ mice with *Tie2-Cre* transgenic mice. The creation of Gab2KO (*Gab1*$^{flox/flox}$ Gab2$^{-/-}$) mice were also described previously.[11] All the animals used for the experiments were 7- to 8-week-old male mice maintained on a 129/Sv-C57BL/6J-CD-1 mixed background. We housed all animals in a virus-free facility on a 12-hour light/12-hour dark cycle and fed them a standard mouse food. All experiments were carried out under the guidelines of Osaka University Committee for animal and rDNA experiments and were approved by the Osaka University Institutional Review Board.

Results

Generation of Endothelium-Specific Gab1 Knockout Mice

To elucidate the functional role of Gab1 in the endothelium, we first generated Gab1ECKO mice using the *Cre-loxP* system. We created a *Gab1*^{flox} allele by introducing 2 *loxP* sites into introns flanking exon 2 which encodes part of the pleckstrin homology domain as described previously.[11] To cause recombination of the floxed allele exclusively in EC lineage, mice homozygous for the *Gab1-loxP*-targeted allele (*Gab1*$^{flox/flox}$) were crossed with transgenic mice expressing *Tie2* promoter-driven *Cre* recombinase (*Tie2-Cre* mice).[23] We created Gab1ECKO (*Gab1*$^{flox/flox}$ Tie2-Cre(+)) mice by crossing

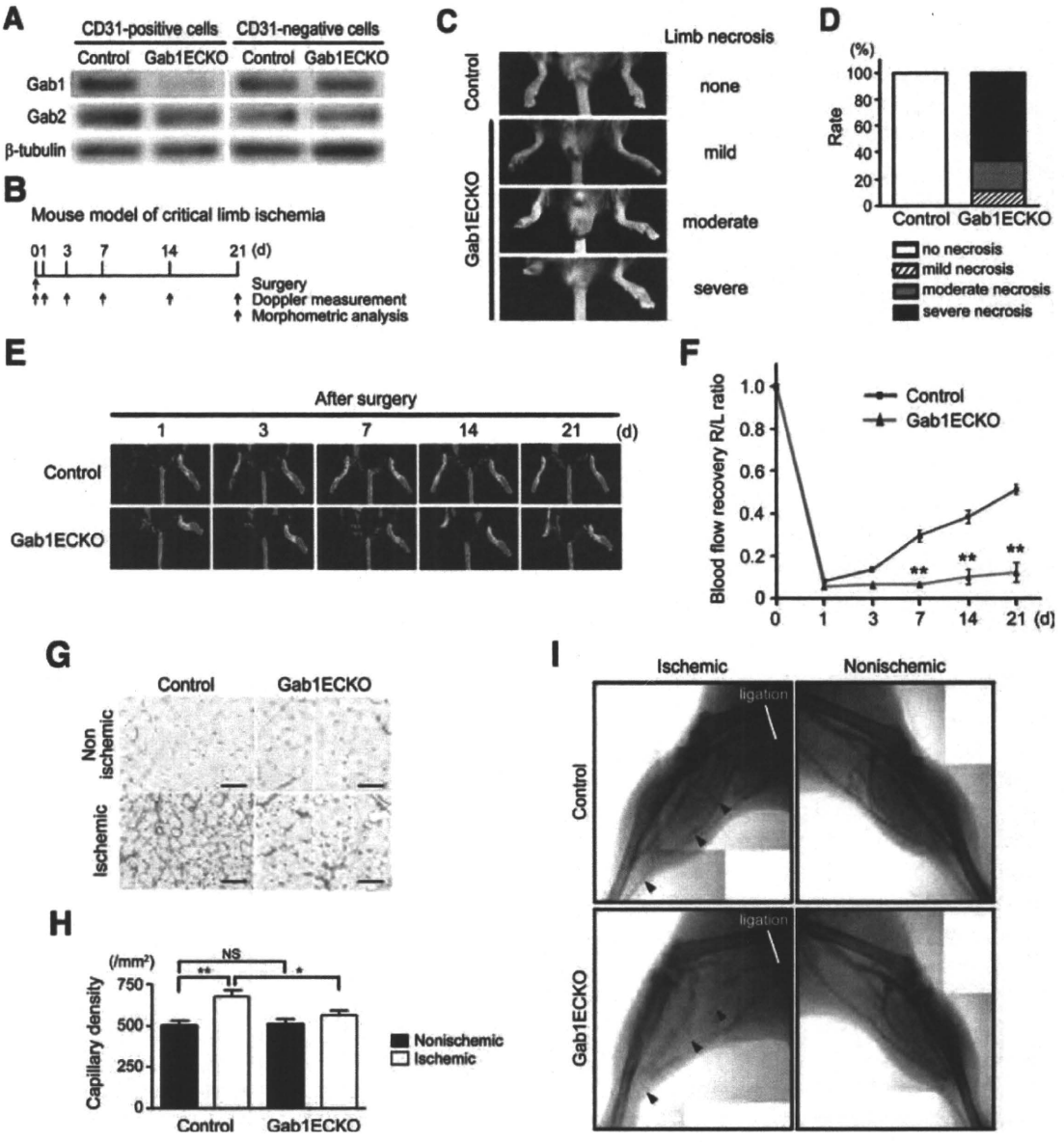

Figure 1. Impaired blood flow recovery and angiogenesis in Gab1ECKO mice. A, Gab1 was successfully ablated in the ECs in Gab1ECKO mice. The CD31-positive ECs were purified from the limb muscles using the MACS system. Whereas the expression of both Gab1 and Gab2 in the CD31-negative cells was almost comparable between the 2 groups, the expression of Gab1 was exclusively depleted in the CD31-positive cells in Gab1ECKO, but not in control mice. The expression levels of both Gab2 and β-tubulin were comparable between 2 groups. **B,** HLI was induced and blood flow of ischemic **(right)** and nonischemic **(left)** limb were measured on gastrocnemius muscle before and on the indicated days after surgery using LDBF analyzer. Tissues were harvested on day 21. **C,** All of Gab1ECKO mice showed limb necrosis after HLI, whereas control mice displayed no necrosis. **D,** Gross morphology of the ischemic limb was assessed on day 21 after surgery. **E,** Representative LBDF images of a mouse HLI on day1, 3, 7, 14, and 21 after surgery. **Red** represents greater flow; **blue,** less flow. **F,** Quantitative analysis of blood flow recovery after HLI expressed as ischemic **(right)** to nonischemic **(left)** LDBF ratio in control (n=9) and Gab1ECKO mice (n=9). Values are shown as means±SEM. $^{**}P<0.01$ vs control. **G,** Representative CD31 staining of capillaries from sections of nonischemic and ischemic adductor muscles. **Scale bar,** 100 μm. **H,** Quantitative analysis of capillary density in control and Gab1ECKO mice (number per high-power field; ×400 magnification). Values are shown as means±SEM. $^{*}P<0.05$, $^{**}P<0.01$ for the indicated groups. **I,** Arteriogenesis was determined by barium sulfate casting followed by x-ray microangiography. Three weeks after femoral artery ligation, mice were anesthetized and subjected to barium sulfate perfusion. Collateral artery growth is significantly attenuated in Gab1ECKO mice compared with control mice as indicated by arrowheads.

Gab1$^{+/flox}$ Tie2-Cre(+) mice with *Gab1*$^{flox/flox}$ mice. The offspring of these crossings were obtained at expected Mendelian ratios as follows: *Gab1*$^{flox/flox}$ Tie2-Cre(+) (n=23; 24.5%); *Gab1*$^{flox/flox}$ (n=27; 28.7%); *Gab*$^{+/flox}$ Tie2-Cre(+) (n=24; 25.5%); *Gab1*$^{flox/flox}$ (n=20; 21.3%).

To confirm the knockout of Gab1 protein in the vascular endothelium, the CD31-positive ECs were purified from the limb muscles of control (*Gab1*$^{flox/flox}$) and Gab1ECKO mice using the Magnetic Cell Sorting (MACS) system (Miltenyi Biotec Inc). The lysates of either purified CD31-positive ECs or CD31-negative cells were subjected to immunoblotting analyses. We confirmed successful depletion of Gab1 protein in CD31-positive ECs derived from Gab1ECKO mice, but not from control mice (Figure 1A). We also confirmed that

Gab1 expression in CD31-negative cells was almost comparable between control and Gab1ECKO mice (Figure 1A). There was no significant difference in Gab2 expression between control and Gab1ECKO mice both in CD31-positive ECs and CD31-negative cells (Figure 1A).

Next, we examined whether Gab1ECKO mice show vascular developmental abnormalities by whole-mount immunohistochemical staining with anti-CD31 antibody. Gab1ECKO mice did not show any obvious developmental vascular defects both during embryogenesis and at 8 weeks of age compared with control mice (Online Figure I, A through H). In addition, we crossed control ($Gab1^{flox/flox}$) mice with $Gab2^{-/-}$ mice to create $Gab1^{flox/flox}$ $Gab2^{-/-}$ mice, designated as Gab2KO mice. Gab2KO mice did not show any obvious vascular developmental defects at birth almost similarly as Gab1ECKO mice (data not shown).

Gab1 in the Vascular Endothelium Is Essential for Postnatal Angiogenesis and Arteriogenesis After Ischemia

To determine the role of Gab1 and Gab2 in postnatal angiogenesis, control, Gab1ECKO, and Gab2KO male mice were subjected to HLI that was created by unilateral femoral artery ligation and analysis at different time points as diagrammed in Figure 1B. From day 7 to 21 after surgery, all of Gab1ECKO mice showed various grades of limb necrosis, whereas no necrotic phenotypes were observed in control and Gab2KO mice (Figure 1C and 1D; Online Figure II, A and B). To precisely determine functional defects in Gab1ECKO mice, blood flow of ischemic and nonischemic limb perfusion were measured before and on 1, 3, 7, 14, and 21 days after surgery using laser Doppler blood flow (LDBF) analyzer. Blood flows on the basal condition and on day 1 after surgery were comparable among mice from each group. Compared with the nonischemic limb, blood flow recovery of the ischemic limb was also comparable between control and Gab2KO mice (Online Figure II, C and D). These findings indicate that Gab2 is not critically engaged in blood flow recovery after HLI. In clear contrast, blood flow recovery in Gab1ECKO mice was substantially impaired on 7, 14, and 21 days (Figure 1E and 1F). These results indicate that endothelial Gab1 has a crucial role for blood flow recovery in response to HLI.

The improvement in blood flow recovery mainly corresponds to increased tissue capillary densities on day 21 after HLI (Figure 1G and 1H). The capillary densities in the nonischemic adductor muscles were comparable between control and Gab1ECKO mice (Figure 1G and 1H). On the other hand, control mice showed increased capillary densities in the ischemic adductor muscles, whereas Gab1ECKO mice exhibited no significant increase in capillary densities (Figure 1G and 1H). These findings indicate that Gab1, but not Gab2, has an essential role for blood flow recovery via the angiogenic response to HLI.

We also examined ischemia-initiated arteriogenesis in control and Gab1ECKO mice by barium sulfate casting followed by x-ray angiographic analysis. Interestingly, Gab1ECKO mice showed a significantly attenuated collateral formation compared with control mice (Figure 1I). These data suggest that Gab1 might have a critical role not only in angiogenesis but also in arteriogenesis after HLI.

HGF Induces the Strongest Tyrosine Phosphorylation of Gab1 and Gab2 in the ECs

Several proangiogenic factors have been reported to regulate angiogenesis after ischemia. To elucidate how Gab1 is involved in the angiogenic response in the vascular endothelium, we performed in vitro experiments using human umbilical vein ECs (HUVECs). We first examined the expression of Gab family transcripts by RT-PCR and detected the mRNA of Gab1 and Gab2, but not that of Gab3 in HUVECs and human aortic ECs (Figure 2A). To examine which ligand induces tyrosine phosphorylation of Gab1 in HUVECs, cells were stimulated with proangiogenic factors such as HGF, VEGF, and fibroblast growth factor (FGF)2. Among these, HGF induced the strongest tyrosine phosphorylation of Gab1 and the subsequent complex formation of Gab1 with SHP2 and p85 in HUVECs (Figure 2B). We confirmed this result using 2 antibodies recognizing Gab1 only if phosphorylated on Tyr-627 or Tyr-307. Figure 2D and 2E show that both residues are strongly phosphorylated in response to HGF stimulation of HUVECs. We also examined the tyrosine phosphorylation of Gab2, another Gab family protein expressed in HUVECs, after stimulation with HGF, VEGF, or FGF2. HGF induced strong tyrosine phosphorylation of Gab2 and the subsequent complex formation of Gab2 with SHP2 and p85 in HUVECs, almost similarly as that of Gab1 (Figure 2C). Thus, Gab1 and Gab2 undergo strong tyrosine phosphorylation on HGF stimulation, suggesting that Gab1 and Gab2 might have a role for HGF-dependent signaling in HUVECs.

We also examined activation of downstream signaling pathways of Gab proteins after stimulation with HGF, VEGF, or FGF2. Among these, HGF induced the strongest and the most sustained activation of ERK1/2 and AKT in HUVECs (Figure 2D, 2F, and 2G). We previously reported that Gab1 is critically involved in activation of ERK5 after stimulation with leukemia inhibitory factor in cardiomyocytes.[18,19] Therefore, we performed ERK5 in vitro kinase assay using glutathione *S*-transferase (GST) fusion protein containing transactivating domain of myocyte enhancer factor 2 (MEF2C) (GST-MEF2C) as a substrate. HGF induced the strongest activation of ERK5 in HUVECs among these agonists (Figure 2H and 2I). Collectively, HGF induces the strongest activation of ERK1/2, AKT, and ERK5 in HUVECs, indicating that Gab family proteins might have an important role for full activation of these downstream pathways in HUVECs.

Gab1, But Not Gab2, Is Required for Activation of ERK1/2, AKT, and ERK5 After Stimulation With HGF in HUVECs

To examine the role of Gab1 and Gab2 in HGF-dependent signaling pathway, we performed small interfering (si)RNA-mediated knockdown of Gab1 and Gab2 in HUVECs. We observed successful depletion of Gab1 or Gab2 protein in HUVECs 48 hours after transfection with the Gab1- or Gab2-specific siRNA, respectively (Figure 3A). The speci-

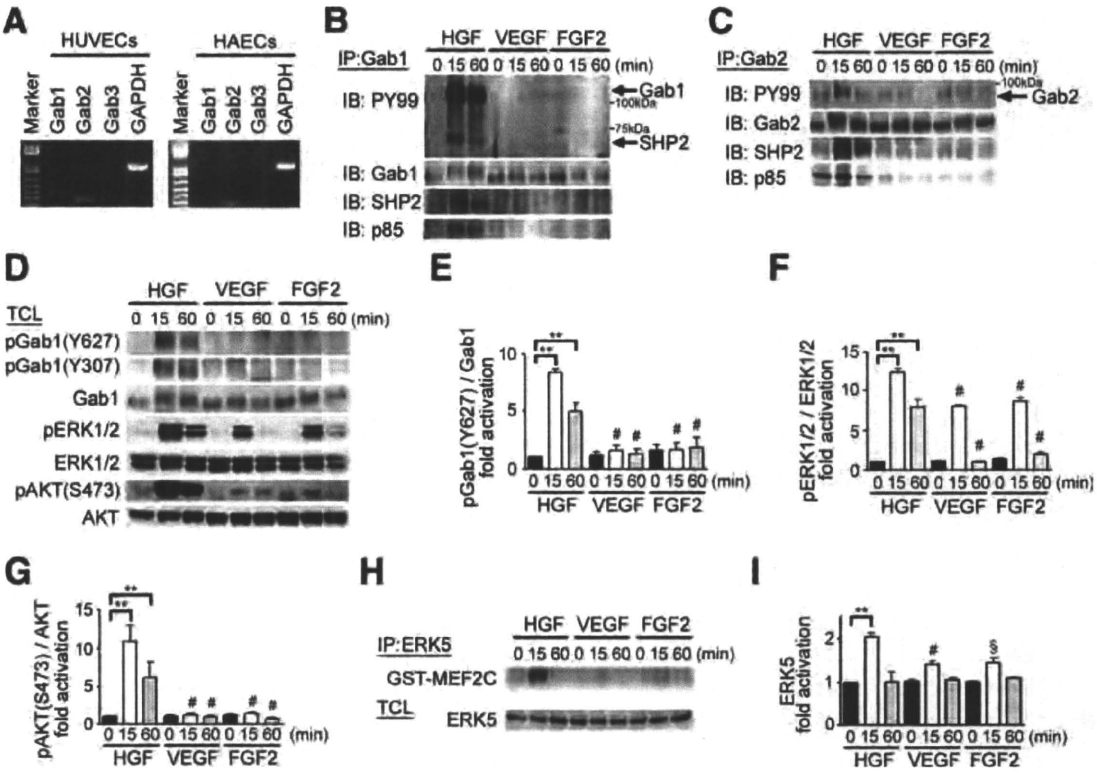

Figure 2. Gab1 and its downstream signaling pathways are strongly activated after stimulation with HGF in HUVECs. A, RT-PCR shows the expression of Gab1 and Gab2 mRNAs, but not Gab3 mRNA, in both HUVECs and human aortic ECs (HAECs). **B and C,** Tyrosine phosphorylation of Gab1 **(B)** and Gab2 **(C)** and their association with SHP2 and p85 were analyzed by immunoprecipitation of the HUVECs lysates. HUVECs were stimulated with HGF, VEGF, or FGF2 and cell lysates were subjected to immunoprecipitation with anti-Gab1 **(B)** or anti-Gab2 **(C)** serum, followed by immunoblotting analysis using the antibodies indicated at the **left. D,** Phosphorylation of Gab1 on Tyr-627 or Tyr-307, ERK1/2, and AKT were assessed by phosphor-specific antibodies. **E,** Phosphorylation of Gab1 on Tyr-627 was quantified against total Gab1 (n=3). **F,** Phosphorylation of ERK1/2 was quantified against total ERK1/2 (n=3). **G,** Phosphorylation of AKT (Ser473) was quantified against total AKT (n=3). **H,** ERK5 activity was measured by in vitro kinase assay using anti-ERK5 immunoprecipitates from the corresponding cell lysates as described in Methods (n=3). ^{32}P-labeled substrates are shown at the **top** (GST-MEF2C). In parallel, cell lysates were subjected to immunoblotting with anti-ERK5 antibody **(bottom)** to confirm the equal amount loading. **I,** ERK5 activity was quantified by scanning densitometry and was expressed relative to input ERK5 (total cell lysate). The results were expressed as relative intensity over cells treated with vehicle. $^{**}P<0.01$ for the indicated groups; $\#P<0.01$, $\S P<0.05$ vs HGF-treated cells at the same time after stimulation. Values are shown as means±SEM for 3 separate experiments.

ficity of this inhibition was demonstrated by the unaltered expression of ERK1/2 and AKT in each condition (Figure 3A). HGF-induced activation of ERK1/2, AKT, and ERK5 were significantly attenuated in HUVECs transfected with Gab1-specific siRNA compared with those transfected with control siRNA (Figure 3A through 3E). Conversely, HGF-induced activation of ERK1/2, AKT, and ERK5 were significantly enhanced in HUVECs transfected with Gab2-specific siRNA compared with those transfected with control siRNA (Figure 3A through 3E), suggesting that Gab2 might exert an inhibitory role for HGF/c-Met/Gab1-dependent signaling. These data indicate that Gab1 and Gab2 might have an opposite role for activation of ERK1/2, AKT, and ERK5 after HGF stimulation in HUVECs.

Gab1 Has an Essential Role for HGF-Dependent Signaling Through Association With SHP2 and p85 in HUVECs

To delineate the role of Gab1 in HGF-dependent signaling, we used adenovirus vectors expressing β-galactosidase (β-gal) (control), wild-type Gab1 ($Gab1^{WT}$), mutated Gab1 that is unable to bind SHP2 ($Gab1^{\Delta SHP2}$), or mutated Gab1 that is unable to bind p85 ($Gab1^{\Delta p85}$), as described previously.[18,24] We found that Gab1 indeed associated with c-Met after stimulation with HGF in HUVECs overexpressing $Gab1^{WT}$ (Online Figure III). Next, we examined the effect of adenovirus-mediated forced expression of $Gab1^{WT}$, $Gab1^{\Delta SHP2}$, or $Gab1^{\Delta p85}$ on the HGF-dependent downstream signaling pathways. HGF induced activation of ERK1/2, AKT, and ERK5 in the control HUVECs expressing β-gal (Figure 4A and 4D). Whereas HGF-induced activation of ERK1/2 was augmented in HUVECs expressing $Gab1^{WT}$ or $Gab1^{\Delta p85}$ compared with control cells expressing β-gal, activation of ERK1/2 was significantly attenuated in HUVECs expressing $Gab1^{\Delta SHP2}$ (Figure 4A and 4B). Furthermore, HGF-induced activation of ERK5 was enhanced in HUVECs expressing $Gab1^{WT}$ compared with control cells expressing β-gal. In addition, enhanced activation of ERK5 was abrogated in HUVECs expressing $Gab1^{\Delta SHP2}$ compared with cells expressing $Gab1^{WT}$ (Figure 4D and 4E). Therefore, the complex formation of Gab1 with SHP2 is required not only for activation of ERK1/2 but also for that of ERK5 after stimulation with HGF in HUVECs.

On the other hand, HGF-induced activation of AKT was significantly enhanced in HUVECs expressing $Gab1^{WT}$ or